

Reply to Reviewer #2 comments on “Theoretical study of mixing in liquid clouds – Part 1: Classical concept” by A. Korolev et al.

Authors appreciate the Reviewer’s comments and time to read the manuscript. Special thank for the careful reading of our manuscript.

1. page 3, Line 70: Beals et al 2015 not 2016

Reply: The year of the reference Beals et al. 2015 was adjusted in line 70 of the revised manuscript.

2. page 10: N_0 in Equation 16a and 17a should be N_1

Reply: The variable N_0 in equations 16a and 16b (page 10) was corrected to N_1 as per Reviewer’s comment. Thank you for noticing it.

3. page 12, Line 318: Pinsky et al. 2015 a b should be 2016. or change others back to 2015 in the paper (for example, page 4, Line 110). Check references page 29... same authors, title, different years.

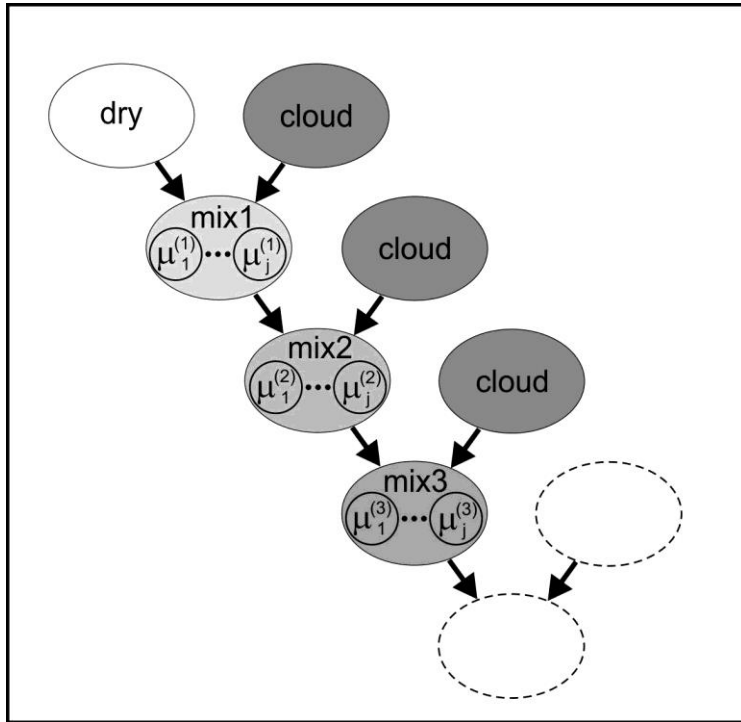
Reply: The year of Pinsky et al. 2016 was adjusted as per Reviewer’s comment throughout the text (lines 110, 111, 317, 484, 524, 620, 654, 810, 813). We also fixed years of the references Squires, 1952 (page 10, line 279), Su et al. 1998 (page 3, line 62)

4. page 16, Line 431: add "homogeneous" between "progressive" and "mixing"

Reply: Corrected as per reviewer’s comment (page, 16, line 431).

5. Figure 10 is confusing. The description of figure 10 (page 16, Line 438-448) is correct, but not consistent with Figure 8. Figure 10 discusses the mixing between two mixed parcels, for example, A mixed with C. However, Figure 8 illustrates the mixing between an undiluted cloud parcel with a mixed parcel, which in the figure should be O mixed with A or C. Please clarify the progressive mixing in the paper. Does it consider the mixing between mixed parcels? Or does it only consider mixing between mixed parcel and original cloud parcel.

Reply: The confusion is probably caused by that the diagram in Figure 8 shows result of mixing marked by ‘MIX1’, ‘MIX2’, ‘MIX3’ as one circle, which may be associated with a single mixed parcel having same microphysical properties thought its volume. In our consideration the progressive model assumes that mixing at any stage results in an ensemble of elementary volumes from mixing of the entrained and cloud volumes with different $\mu_j^{(n)}$. In order to make the description of progressive mixing more clear the following text was added on page 16 (lines 418-420): “Each stage of mixing results in an ensemble of elementary parcels formed for different $\mu_j^{(n)}$. The elementary parcels continue mixing with each other and cloud environment during the subsequent mixing stages.”. Figure 8 was also modified in order to show that mixing results in multiple elementary volumes. The modified Figure 8 is shown below.



6. page 17, Line 464: add "extreme" before "inhomogeneous mixing"

Reply: Corrected as per reviewer's comment (page, 16, line 434).

7. page 17, Line 473: is it because always mixing with original cloud parcel? This is related to comment 5. I still find this confusing.

Reply: As mentioned in Comment 5 we expanded the explanation of progressive mixing in the text and modified Figure 8. We hope this would help mitigating the confusion.

8. Figure 5, what are q and T when changing RH (a,b,c), what are RH_2 and T when changing q_1 (d,e,f), and what are q_1 and RH_2 when changing T (g,h,j)?

Reply: The following text was added in the caption of Figure 5 in order to address the Reviewer's comment: "The calculations were performed the initial conditions: $H=1000\text{m}$, $D_1=20\mu\text{m}$; for (a-c) $T_1 = T_2 = 0\text{C}$, $N_1=500\text{cm}^{-3}$; (d-f) $T_1 = T_2 = 0\text{C}$, $RH_2 = 0.5$; (g-j) $T_1 = T_2 = T$, $N_1=500\text{cm}^{-3}$, $RH_2 = 0.5$."

1 **Theoretical study of mixing in liquid clouds. Part 1: classical concepts**

2

3 (revised version, ~~14 March~~21 May 2016)

4

5 **Alexei Korolev¹, Alex Khain², Mark Pinsky², and Jeffrey French³**

6 [1] Environment Canada, Cloud Physics and Severe Weather Section, Toronto, Canada

7 [2] Department of Atmospheric Sciences, the Hebrew University of Jerusalem, Israel

8 [3] University of Wyoming, Laramie, WY, USA

9 Correspondence to: A. Korolev (alexei.korolev@canada.ca)

10

11

12

13 **Abstract**

14 The present study considers final stages of in-cloud mixing in the framework of classical concept
15 of homogeneous and extreme inhomogeneous mixing. Simple analytical relationships between basic
16 microphysical parameters were obtained for homogeneous and extreme inhomogeneous mixing
17 based on the adiabatic consideration. It was demonstrated that during homogeneous mixing the
18 functional relationships between the moments of the droplets size distribution hold only during
19 primary stage of mixing. Subsequent random mixing between already mixed parcels and undiluted
20 cloud parcels breaks these relationships. However, during extreme inhomogeneous mixing the
21 functional relationships between the microphysical parameters hold both for primary and subsequent
22 mixing. The obtained relationships can be used to identify the type of mixing from in situ
23 observations. The effectiveness of the developed method was demonstrated using in-situ data
24 collected in convective clouds. It was found that for the specific set of in-situ measurements the
25 interaction between cloudy and entrained environments was dominated by extreme inhomogeneous
26 mixing.

27

28

29

30

31 **1 Introduction**

32 Turbulent mixing is an important non-adiabatic process in the atmosphere that to a large extent
33 determines spatial gradients of many thermodynamic (e.g. temperature, humidity) and cloud
34 microphysical parameters (e.g. hydrometeor concentrations, extinction coefficient, condensed water
35 content) and as such, needs to be properly described in numerical simulations of clouds and weather
36 predictions. Entrainment and mixing occurs during the entire lifetime of a cloud and is active not
37 only near cloud edges, but it is important throughout the whole cloud volume. Mixing of cloudy and
38 entrained air results in changes to the shape of the droplet size distribution through partial droplet
39 evaporation and can also lead to changes in droplet concentration through complete evaporation of
40 some fraction of droplets and dilution. The shape of the droplet size distribution plays key role in the
41 initiation of precipitation and radiative properties of clouds.

42 The treatment of mixing in numerical simulations of clouds and precipitation formation remains
43 a challenging problem. Besides the issues related to the way to describe mixing in numerical
44 schemes, there is a fundamental problem of identifying a scenario or path, that mixing events should
45 follow. Through the pioneering works of Latham and Reed (1977) and Baker et al. (1980) two
46 explicitly alternative scenarios of mixing were identified. In the first scenario turbulent mixing
47 rapidly stirs the environment homogenizing the fields of temperature and humidity. Following that,
48 all of the droplets undergo partial evaporation under the same conditions. The result of this mixing
49 is a droplet population with reduced sizes, but a total number ~~that of droplets~~ remains unchanged.
50 This type of mixing is referred to as *homogeneous*. In the second scenario mixing occurs more slowly
51 such that the population of droplets experiences different amount of sub-saturation. Some number
52 of droplets completely evaporates, while others experience no evaporation until the entirety of the
53 entrained air becomes saturated. Following that, turbulence mixes the rest of the droplets with the
54 saturated, but droplet-free environment. During this type of mixing the size of droplets remains
55 unchanged; however, their total number is reduced. This type of mixing is called *extreme*
56 *inhomogeneous*. The intermediate case when some fraction of droplets evaporates partially, another
57 other fraction evaporates completely, and a third fraction remains unchanged is in some works
58 referred to as inhomogeneous (e.g. Baker and Latham, 1980).

59 The conditions for homogeneous and extreme inhomogeneous mixing and their effects on
60 precipitation formation have been debated in cloud physics over forty years. There are a number of
61 numerical simulations and theoretical efforts on studying different aspects of mixing and its effect

62 on cloud microphysics (e.g. Baker and Latham, [1979](#), 1982; Jensen and Baker, 1989; [Su et al.](#),
63 [1989](#)[1998](#); Lasher-Trapp et al., 2005; Jeffrey, 2007; Andrejczuk et al., 2009; Kumar et al., 2013;
64 Jarecka et al., 2013; [Lu et al. 2011, 2014](#); [Tolle and Krueger 2014](#); and many others). A
65 comprehensive review of the works on the effect of turbulence and mixing on cloud droplet
66 formation can be found in Devenish et al. (2012).

67 A number of studies were dedicated to identifying type of mixing based on in-situ observations.
68 Most of the previous observations provided evidence supporting inhomogeneous mixing (e.g. Hill
69 and Choulaton, 1985; Paluch, 1986; Bower and Choulaton, 1988; Blyth and Latham, 1991; Gerber
70 et al., 2008, Lu et al. 2011; [Beals et al. 2016](#)[2015](#)). However, works of Jensen and Baker (1989),
71 Paluch and Baumgardner (1989), Burnet and Brenguier (2007), Lehmann et al. (2009), Lu et al.
72 (2011) suggested occurrence of homogeneous mixing. So, at the moment it appears that both types
73 of mixing may occur in liquid clouds. However, the environmental conditions governing one or the
74 other type of mixing remain not well understood.

75 Early experimental work on identifying type of mixing from in-situ observations were based on
76 the analysis of spatial variability of the shapes of individual droplet size distributions (e.g. Paluch
77 and Knight, 1984; Paluch, 1986; Bower and Choulaton, 1988). The effectiveness of this method
78 involving the analysis of a large number of individual size spectra turned out to be quite low. Another
79 technique utilized expected functional relationships between droplet concentration (N) and droplet
80 diameter (D) specific to each type of mixing. Thus, during extreme inhomogeneous mixing the
81 droplet size is expected to remain unchanged, whereas the concentration will vary. During
82 homogeneous mixing the droplet size and concentration in cloud will be related to each other in a
83 certain way, depending on the mixing fraction and the humidity of the entrained air. This fact was
84 used in observational studies for identifying the type of mixing from “mixing diagrams” that related
85 N and D_v for different regimes of mixing (e.g. Burnet and Brenguier, 2007; Gerber et al., 2008;
86 Lehmann et al., 2009).

87 The use of mixing diagrams to some extent facilitated identification of type of mixing. However,
88 in many cases scatter in the relationships between N vs. D_v was too large, hindering identification of
89 the type of mixing (Burnet and Brenguier, 2007). To resolve this problem many researchers used
90 other complementary measurements supporting identification of the type of mixing (e.g. Gerber et
91 al., 2008; Lehmann et al., 2009).

92 Besides the effect on N and D_v , the type of mixing is anticipated to manifest itself in relationships
93 between other moments of the droplet size distribution, $f(D)$. Such relationships may provide insight
94 into the mixing process and identify type of mixing. With the exception of the work by Hill and
95 Choulaton (1985), who correlated concentration and liquid water content, there have been few
96 attempts to use any other microphysical parameters for identification of type of mixing.

97 In order to fill this gap, this study presents a theoretical analysis of relationships between
98 different moments of $f(D)$ within the framework of homogeneous and extreme inhomogeneous
99 mixing. The analysis is focused on the first four moments of $f(D)$ corresponding to the droplet
100 concentration N (0th moment), integral diameter $N\bar{D}$ (1st moment), extinction coefficient β (2nd
101 moment), liquid water mixing ratio q (3rd moment) and mean volume diameter D_v (mixed 3rd and 0th
102 moment). It is shown that the newly obtained relationships between the moments provide a more
103 robust identification of type of mixing from in-situ measurements as compared to conventional $N -$
104 D_v^3 relationships used in mixing diagrams. Relationships between moments may be useful for
105 parameterization of mixing in numerical simulations of clouds and climate, interpretations of remote
106 sensing measurements.

107 This paper constitutes the first in a series of three papers. It considers the final stage of mixing
108 based on the formal definitions of homogeneous and extreme inhomogeneous mixing. These two
109 types of mixing present two extreme regimes of mixing. The following two papers provide a
110 detailed analysis of the time dependent processes during homogeneous (Pinsky et al., 2015a2016a)
111 and inhomogeneous (Pinsky et al., 2015b2016b) mixing where non-extreme regimes are
112 considered as well.

113 This paper is arranged in the following way. Section 2 presents analysis of the analytical
114 relationship between N , $N\bar{D}$, β , q , D_v and mixing fraction μ for the cases of homogeneous and
115 extreme inhomogeneous mixing. In Sect. 3 the obtained analytical relationships are compared with
116 the ~~results of numerical simulations~~ of N , β , q , D_v formed at the final stage of mixing.
117 Section 4 presents results of simulation of progressive mixing and ~~its~~ effect of the relationships
118 between moments. Examples of relationship between N , β , q and D_v from in-situ observations are
119 ~~presented~~ provided in Sect. 5. The discussion and concluding remarks are presented in Sect. 6 and 7.
120

121 2 Effect of mixing on microphysical variables

122 2.1 Phenomenological consideration

123 The conceptual diagrams of homogeneous and extreme inhomogeneous mixing are shown on
124 Fig. 1. During the first stage of extreme inhomogeneous mixing the subsaturated parcel is engulfed
125 into the cloudy environment (Fig. 1a1). Then, the droplets at the interface of the sub-saturated parcel
126 and the cloud environment undergo complete evaporation until the air within the engulfed volume
127 reaches saturation (Fig. 1a2). After that the saturated but droplet free parcel mixes with the rest of
128 the cloud environment (Fig. 1a3). The result of inhomogeneous mixing is that the cloud parcel has
129 reduced droplet concentration and the droplet sizes remain unchanged.

130 In the case of homogeneous mixing after entraining into a cloud (Fig. 1b1), the subsaturated
131 parcel “instantly” mixes up with its cloud environment (Fig. 1b2) leading to undersaturation of the
132 total volume. Then, all droplets throughout the mixed volume undergo simultaneous evaporation
133 until the equilibrium state is reached. The result of homogeneous mixing is a cloud volume with
134 reduced concentration of droplets and droplets with reduced sizes (Fig. 1b3).

135 Based on mass and energy conservation the final state of the bulk parameters (i.e. liquid water
136 mixing fraction, humidity, temperature, etc.) is the same for both types of mixing. However, in the
137 case of extreme inhomogeneous mixing saturation is reached through complete evaporation of some
138 fraction of droplets, and their sizes remain constant. Whereas in case of homogeneous mixing
139 saturation is reached through a uniform evaporation of droplets, and the total number of droplets
140 remains unchanged. It should be noted, that in both cases the droplet concentration decreases due to
141 dilution by the mixed droplet free sub-saturated parcel.

142 The following discussion will be specifically focused on the microphysical properties formed at
143 the final stage of the homogeneous and extreme inhomogeneous mixing. The processes occurring
144 during mixing state (i.e. transition 1a→2a and 1b→2b in Fig. 1) remain outside the frame of this
145 work. Following the formalism of homogeneous and extreme inhomogeneous mixing, the process of
146 mixing reaches the final stage when (1) the entrained and cloud environment are mixed up and the
147 spatial gradients of the microphysical (N , β , q , etc.) and environmental (T , S , e , etc.) parameters
148 approach to zero; (2) the diffusional process related to droplet evaporation comes into equilibrium.
149 The second condition is completed when (a) the environment reaches saturation state, or (b) the entire
150 population of droplets is completely evaporated, if the entrained air is sufficiently dry.

151 The above description of homogeneous and extreme inhomogeneous mixing is highly idealized.
152 Actual in-cloud mixing does not occur as a sequence of discrete events (Fig.1) that individually come
153 to equilibrium only to be followed by next discrete mixing events. But rather it is occurring

154 continuously on a cascade of different spatial and time scales. Broadwell and Breidenthal (1982)
155 summarized the experimental evidence and proposed the following description of mixing in turbulent
156 shear layers. Mixing takes place in a series of events. Two shear layers exchange mass by engulfing
157 parcels from an opposite layer into localized zones. The initially large-scale filaments of the two
158 gases break down towards smaller scales due to the action of turbulence. The turbulence stretches
159 the interface between the gases and enhances the molecular diffusion across the increasing surface.
160 The actual mixing of the engulfed volume is a molecular diffusion process that is most effective after
161 the break down volumes reduce to the Kolmogorov viscosity scale. It is anticipated that the reaction
162 of the ensemble of droplets is a combination of homogeneous and inhomogeneous mixing with
163 domination of one type of mixing over the other depending on the characteristic spatial and time
164 scales of the environment determined by turbulence, cloud microphysics, state parameters and stage
165 of mixing.

166

167 **2.2 Methodology**

168 The foregoing discussion will be focused on mixing between saturated cloud parcels and out-
169 of-cloud sub-saturated air. The cloud parcel contains droplets with average diameter \bar{D}_1 , liquid
170 mixing ratio q_1 and number concentration N_1 . The initial temperature in the cloud parcel is T_1 ,
171 relative humidity $RH_1 = 1$, where $RH = e/e_s(T)$ (the explanation of variable notations is provided
172 in Table 1). The second parcel is droplet free ($N_2 = 0$), sub-saturated with initial relative humidity
173 $RH_2 < 1$ and temperature T_2 . The mixing occurs isobarically, i.e. $p = \text{const}$. At the final stage of
174 mixing the temperature and humidity formed in the resulting parcel are T and RH (appendix A). The
175 process of mixing is completed when the mixed parcel reaches equilibrium due to the air saturation
176 (i.e. $RH = 1$) or due to the complete evaporation of droplets. In the latter case the final humidity is
177 $RH \leq 1$. The effect of the vertical velocity and vertical travel on final T , RH , and q is not considered
178 here, i.e. vertical velocity $u_z = 0$.

179 Without the loss of generality the masses of the cloudy and sub-saturated volumes prior to the
180 mixing are assumed to have a unit masses, i.e. $m_1 = 1$ and $m_2 = 1$. The mixing process will be
181 considered as mixing of μ fraction of the cloud parcel with $(1 - \mu)$ fraction of the second (sub-
182 saturated) parcel. The mixing cloud fraction may vary within the range of $0 \leq \mu \leq 1$. Therefore, the
183 mass of the resulting mixed parcel is equal to $m_1\mu + (1 - \mu)m_2 = 1$. This approach simplifies the

184 consideration of mixing and allows considering all possible proportions of the mixing of two
 185 volumes.

186

187 **2.3 Effect of mixing on liquid water and temperature**

188 The mixing ratio of liquid water q formed at the final stage of mixing is determined by the mass
 189 of the mixing cloud water μq_1 and amount of evaporated water required to saturate the newly formed
 190 mixed volume δq_m . The mass balance of liquid water for the mixing volume yields

$$191 \quad q = \mu q_1 - \delta q_m, \quad (1)$$

192 where

$$193 \quad \delta q_m = \frac{c_p R_v T_{m0}^2}{L^2} \ln \left(\frac{1 + \frac{e_s(T_{m0}) R_a L^2}{p c_{pa} R_v^2 T_{m0}^2}}{1 + RH_{m0} \frac{e_s(T_{m0}) R_a L^2}{p c_{pa} R_v^2 T_{m0}^2}} \right) \cong -\frac{S_{m0}}{A_2} \quad (2)$$

194 is the mixing ratio of liquid water required to saturate 1kg of volume with temperature T_{m0} and
 195 humidity RH_{m0} (appendix A); T_{m0} , RH_{m0} and S_{m0} , are the temperature, relative humidity ~~formed~~
 196 and supersaturation formed in the volume after instantaneous air mixing, but before droplets start
 197 evaporating (appendix A); $e_s(T_{m0})$ is saturation vapor pressure at temperature T_{m0} .

198 Eq. (1) is a non-linear function of μ , since T_{m0} , e_{m0} and thus δq_m ~~depend~~ depends on μ . Eq.(1)
 199 can be simplified, if $T_1 = T_2$. In this case $T_{m0} = T_1 = T_2$, and $e_s(T_{m0}) = e_s(T_1) = e_s(T_2)$. Given
 200 that, the expression under logarithm in Eq.(2) can be expanded in series resulting in (appendix B)

$$201 \quad \delta q_m = (1 - \mu) \delta q^*, \quad (3)$$

202 where

$$203 \quad \delta q^* = \frac{c_p R_v T_2^2}{L^2} \ln \left(\frac{1 + \frac{e_s(T_2) R_a L^2}{p c_{pa} R_v^2 T_2^2}}{1 + RH_2 \frac{e_s(T_2) R_a L^2}{p c_{pa} R_v^2 T_2^2}} \right) \cong -\frac{S_2}{A_2} \quad (4)$$

204 is the mixing ratio of liquid water required to saturate 1 kg of the entrained dry air: with temperature
 205 T_2 and humidity RH_2 . Substituting Eq.(3) in Eq.(1) gives

$$206 \quad q = \mu q_1 - (1 - \mu) \delta q^*, \quad (5)$$

207 The value of δq^* does not depend on μ , and Eq. (5) is a simple linear function of μ . The
 208 comparisons with numerical simulations showed, that Eq.(5) provides accuracy within few percent,
 209 when the temperature difference $|T_1 - T_2| < 2^\circ\text{C}$. Although, in many cases $|T_1 - T_2|$ may vary a
 210 wide range reaching 10°C or higher, clouds with $|T_1 - T_2| < 2^\circ\text{C}$ are quite common. Therefore, for
 211 the sake of simplicity, Eq.(5) and the assumption $T_1 \approx T_2$ will be used in the following consideration
 212 of mixing.

213 It should be noted that, Eqs (1) and (5) are valid for the cases, when $\mu > \mu_{cr}$. Here μ_{cr} is critical
 214 mixing fraction, which separates partial and complete evaporation of cloud water in the mixing
 215 volume (section 2.4). Cases when $\mu \leq \mu_{cr}$ correspond to complete evaporation of droplets, and $q =$
 216 0.

217 The temperature at the final stage of mixing can be estimated as (appendix C)

$$218 \quad T = T_{m0} - \frac{(1-\mu)\delta q^* L}{c_{pa}}, \quad \text{when } \mu > \mu_{cr} \quad (6a)$$

$$219 \quad T = T_{m0} - \frac{\mu q_1 L}{c_{pa}} \quad \text{when } \mu \leq \mu_{cr} \quad (6b)$$

220 Eqs. (1), (5), (6) were obtained based on mass and energy conservation, and they do not depend
 221 on how mixing proceeds. Therefore, Eqs. (1), (5), (6) are valid for both homogeneous and
 222 inhomogeneous mixing.

223

224 **2.4 Complete evaporation**

225 As mentioned in section 2.2 the process of mixing is complete only after reaching equilibrium
 226 by saturating the mixed volume or by evaporating of all cloud droplets depending on the mixing
 227 fraction μ . The critical mixing fraction μ_{cr} , corresponding to evaporation of all droplets, can be found
 228 from Eq.(5) when $q = 0$, i.e.

$$229 \quad \mu_{cr} = \frac{\delta q^*}{q_1 + \delta q^*} \quad (7)$$

230 Critical mixing fraction separates μ in two subranges: (a) $1 \geq \mu > \mu_{cr}$ where q is described by
 231 Eqs.(1) or (5) and $RH_m = 1$; (b) $\mu_{cr} \geq \mu \geq 0$ where $q = 0$ and $RH_m \leq 1$.

232 For the general case when $T_1 \neq T_2$, μ_{cr} , can be found by solving the non-linear equation

$$233 \quad \mu_{cr} q_1 - \delta q_m(\mu_{cr}) = 0 \quad (8)$$

234 Figure 2 shows comparisons of dependences of μ_{cr} vs. q_1 calculated from Eq. (7) and those
 235 deduced from a numerical model (Sect. 3). Critical mixing fraction μ_{cr} is also shown by black stars
 236 in Fig. 4. The locations of the stars in Fig.4 coincide well with the locations, where the modeled
 237 microphysical moments become zero. The obtained agreement between analytical and modeled μ_{cr}
 238 in Figs. 2 and 4 validates the developed approach.

239

240 2.5 Extreme inhomogeneous mixing

241 Within the framework of extreme inhomogeneous mixing some fraction of droplets undergo
 242 complete evaporation, whereas the rest of the droplets remain unchanged. Therefore, such a process
 243 results in scaling the droplet size distribution $f(D)$, i.e.

$$244 \quad f(D) = kf_1(D) \quad (9)$$

245 where k is some coefficient dependent on μ and the initial environmental parameters of the mixing
 246 volumes, $f_1(D)$ is the droplet size distribution before mixing. Equation (9) yields relationships
 247 between pairs n th and m -th moments

$$248 \quad \frac{M_n - M_k}{M_{n1} - M_{k1}} = \frac{M_n}{M_{n1}} = \frac{M_m}{M_{m1}} \quad (10)$$

249 where $M_n = \int_0^\infty f(D)D^n dD / \int_0^\infty f(D)dD$ is the n th moment of $f(D)$. Therefore, it is anticipated that
 250 for extreme inhomogeneous mixing droplet number concentration N (0th moment), extinction
 251 coefficient β (2nd moment), liquid water mixing ratio q (3rd moment), along with other moments,
 252 will correlate with each other, i.e.

$$253 \quad \frac{N}{N_1} = \frac{\beta}{\beta_1} = \frac{q}{q_1} \quad (11)$$

254 One of the consequences of Eqs. (9)-(11) is that the characteristic droplet sizes \bar{D} , D_2 , D_v , D_{eff}
 255 will remain constant during inhomogeneous mixing.

256 For the case $T_1 = T_2$ and $\mu > \mu_{cr}$ Eqs. (5) and (11) yield the dependence of N vs. μ

$$257 \quad N = N_1 \left(\mu - \frac{(1-\mu)\delta q^*}{q_1} \right) \quad (12)$$

$$258 \quad \beta = \beta_1 \left(\mu - \frac{(1-\mu)\delta q^*}{q_1} \right) \quad (13)$$

Field Code Changed

259 For a general case when $T_1 \neq T_2$ the term $(1 - \mu)\delta q^*$ in Eqs. (12) and (13) should be replaced
 260 by $\delta q_m(\mu)$ (Eq.(2)).

261

262 **2.6 Homogeneous mixing**

263 For homogeneous mixing, when $\mu > \mu_{cr}$, the droplet number concentration changes only due to
 264 dilution by the entrained air, i.e.

$$265 \quad \frac{N}{N_1} = \mu \quad (14)$$

266 Assuming $T_1 = T_2$, and substituting Eq. (5) in (14) yields:

$$267 \quad \frac{N}{N_1} = \frac{q + \delta q^*}{q_1 + \delta q^*} \quad (15)$$

268 As follows from Eq. (15) N and q are linearly related for homogeneous mixing. However, no
 269 linear relationships exist between other moments. Thus, substituting the definition of the liquid water
 270 mixing ratio $q = \pi \rho_w N D_v^3 / 6 \rho_a$ in Eq. (15) yields the relationship between mean volume droplet
 271 size ~~and~~ concentration and liquid water mixing fraction

$$272 \quad \frac{D_v^3}{D_{v1}^3} = 1 + \left(1 - \frac{N_0}{N}\right) \frac{\delta q^*}{q_1} \quad \frac{D_v^3}{D_{v1}^3} = 1 + \left(1 - \frac{N_1}{N}\right) \frac{\delta q^*}{q_1}$$

273 (16a)

$$274 \quad \frac{D_v^3}{D_{v1}^3} = \frac{q}{q_1} \left(\frac{q_1 + \delta q^*}{q + \delta q^*} \right) \quad (16b)$$

275 In a similar way the relationship between the extinction coefficient $\beta = Q\pi N D_2^2 / 4$, N and q can
 276 be written as

$$277 \quad \frac{\beta}{\beta_1} = \frac{N}{N_1} \left(1 + \left(1 - \frac{N_0}{N}\right) \frac{\delta q^*}{q_1} \right)^{2/3} \quad \frac{\beta}{\beta_1} = \frac{N}{N_1} \left(1 + \left(1 - \frac{N_1}{N}\right) \frac{\delta q^*}{q_1} \right)^{2/3}$$

278 (17a)

$$279 \quad \frac{\beta}{\beta_1} = \left(\frac{q}{q_1} \right)^{2/3} \left(\frac{q + \delta q^*}{q_1 + \delta q^*} \right)^{1/3} \quad (17b)$$

280 In Eqs. (17a) and (17b) it is assumed that $D_2 \approx D_v$.

Field Code Changed

Field Code Changed

281 Substituting in Eq. (16) the expression for the time of phase relaxation
 282 $\tau_p = 1/bN\bar{D}$ (e.g. Squires 1953, 1952; Korolev and Mazin, 2003) and assuming $\bar{D} \approx D_v$ yields

$$283 \quad \frac{\tau}{\tau_1} = \frac{N_1}{N} \left(1 + \left(1 - \frac{N_1}{N} \right) \frac{\delta q^*}{q_1} \right)^{-1/3} \quad (18)$$

284 For the cases when the temperature difference $|T_1 - T_2|$ exceeds a few degrees, the effect of μ
 285 on T_m and S_m should be taken into consideration in the calculations of evaporated water. For such
 286 cases δq_m (Eq. (2)) should be used instead of δq^* . Using Eq. (14) δq_m can be presented as a function
 287 of $\frac{N}{N_1}$, i.e. $\delta q_m(\mu) = \delta q_m\left(\frac{N}{N_1}\right)$. Replacing Eq. (5) by (1) in the above consideration, the equations
 288 Eqs. (15)-(18) can be rewritten as

$$289 \quad \frac{N}{N_1} = \frac{q + \delta q_m\left(\frac{N}{N_1}\right)}{q_1} \quad (19)$$

$$290 \quad \frac{D_v^3}{D_{v1}^3} = 1 - \frac{\delta q_m\left(\frac{N}{N_1}\right) N_1}{q_1 N} = \frac{q}{q + \delta q_m\left(\frac{q}{q_1}\right)} \quad (20)$$

$$291 \quad \frac{\beta}{\beta_1} = \frac{N}{N_1} \left(1 - \frac{\delta q_m\left(\frac{N}{N_1}\right) N}{q_1 N_1} \right)^{2/3} = \frac{q^{2/3} \left(q + \delta q_m\left(\frac{\beta}{\beta_1}\right) \right)^{1/3}}{q_1} \quad (21)$$

$$292 \quad \frac{\tau_p}{\tau_{p1}} = \frac{N_1}{N} \left(1 - \frac{\delta q_m\left(\frac{N}{N_0}\right) N_1}{q_1 N} \right)^{-1/3} \quad (22)$$

293 Eqs. (19)–(22) can be solved numerically.

294

295 **2.7 Degenerate case**

296 As follows from Eq.(5), if

$$297 \quad \frac{(1-\mu) \delta q^*}{\mu q_1} \ll 1 \quad (23)$$

298 then $q_1 \geq q \gg \delta q^*$. If the condition in Eq. (23) is ~~valid~~satisfied, then the terms associated with δq^*
 299 in Eqs. (15)-(18) can be neglected. This results in correlation of all moments, i.e.
 300 $N/N_1 = \beta/\beta_1 = q/q_1$ (compare with Eq.(11)). This corresponds to the degenerate case, when the
 301 difference between the homogeneous and inhomogeneous mixing vanishes. Thus, the dimensionless
 302 parameter $\xi = \frac{1-\mu}{\mu} \frac{\delta q^*}{q_1}$ in Eq.(23) can be used for characterization of proximity of the homogeneous
 303 mixing moments to those formed during extremelyextreme inhomogeneous mixing.

304 The range of μ in ξ is limited by $\mu_{cr} < \mu \leq 1$, so that $0 < \frac{1-\mu}{\mu} \leq \frac{q_1}{\delta q^*}$. This gives the range of
 305 changes of ξ , i.e. $0 \leq \xi \leq 1$ for the mixing without complete evaporation of all droplets. The
 306 degenerate case corresponds to $\xi \rightarrow 0$, whereas $\xi \rightarrow 1$ corresponds to maximum difference of the
 307 moments for homogeneous and extremelyextreme inhomogeneous mixing.

308 As follows from Eqs. (4) and (23) approaching to the degenerate case ($\xi \rightarrow 0$) occurs, when one
 309 of the following conditions or their combination is satisfied: (a) $RH_2 \rightarrow 1$; (b) $E_s(T) \rightarrow 0$ at low
 310 temperatures; (c) $q_1 \gg \delta q^*$; (d) $\mu \rightarrow 1$. The effect of RH, T, q_1 and μ on mixing will be demonstrated
 311 in Sect.3.

312 Figure 3 shows dependence of ξ vs. μ . The grey area in Fig.3 indicates the region where
 313 identification of type of mixing from in-situ measurements (Sect.5) may be hindered due to proximity
 314 of the moments for homogeneous and extreme inhomogeneous mixing. Thus for $\delta q^*/q_1 = 0.0$
 315 identification of type of mixing is ambiguous for nearly the entire range of μ .

316 For the general case, when $T_1 \neq T_2$, it should be $\xi = \frac{|\delta q_m(\mu)|}{\mu q_1}$. An absolute value $|\delta q_m(\mu)|$
 317 should be used in ξ since $\delta q_m(\mu)$ can be negative (Appendix A, Fig.A1); if mixing results in
 318 supersaturation Sect. 3.4).

319 The coefficient ξ may be useful for identification type of mixing from in-situ observations. It is
 320 worth nothing, that the ratio $\frac{\delta q^*}{q_1} \cong \frac{S_2}{A_2 q_1}$ is equal to the parameter R (Pinsky et al. 2015ab2016ab),
 321 which plays an important role in determining scenarios of droplet evaporation in turbulent
 322 environment.

323 **3 Comparisons with numerical simulations**

324 Numerical simulations were performed to examine accuracy and limitations of the analytical
 325 expressions in Sect.2 and to conduct a sensitivity test to environmental and cloud parameters. The
 326

327 simulations have been performed with the help of a parcel model similar to that in Korolev (1995).
 328 The ensemble of droplets in the simulation was assumed to be monodisperse. For the case of extreme
 329 inhomogeneous mixing the amount of evaporated water Δq required to saturate the mixed volume
 330 was calculated first. If $\Delta q < \mu q_1$, then the concentration of evaporated droplets was calculated as
 331 $N_{ev} = \frac{\Delta q}{m_d} \rho_a$, where $m_d = \pi \rho_w D^3 / 6$. Then, the concentration of the remaining droplets $N = N_1 -$
 332 N_{ev} was recalculated based of the calculation on the volume formed after mixing. If $\Delta q \geq \mu q_1$, then
 333 all droplets evaporate, and $N = 0$.

334 For the case of homogeneous mixing in the first step the engulfed parcel instantly mixes with
 335 the cloud parcel resulting in a new humidity RH_{m0} , temperature T_{m0} and volume V_{m0} . After that the
 336 droplets start evaporating until either their complete evaporation or saturation over liquid is reached.
 337 The calculations stopped when, either $D < 0.2\mu\text{m}$ or $(E_S - e)/E_S < 0.001$, respectively.

338

339 3.1 Effect of mixing fraction

340 Figure 4 shows the results of the simulation of different moments and state parameters vs. μ .
 341 The calculations were performed for different relative humidity of the entrained parcel $RH_2 = 0.2,$
 342 $0.5, 0.8$ and 0.95 . As seen from Fig.4 for the case of homogeneous mixing only N and q are linearly
 343 related with μ , the rest of the variables have non-linear dependences on μ . For the case of extreme
 344 inhomogeneous mixing all $f(D)$ moments and droplet sizes linearly depend on μ . Note, for $\mu \leq \mu_{cr}$
 345 all moments are equal to zero.

346 Since the amount of the evaporated liquid water does not depend on the type of mixing, the
 347 dependences of $q(\mu)$ are the same for both homogeneous and inhomogeneous mixing (Fig.4a). The
 348 type of mixing has the most pronounced effect on the droplet concentration (Fig.4b) and droplet sizes
 349 (Fig.4e).

350 Figure 4g shows the dependences RH_{m0} and RH vs. μ . Here RH_{m0} is the relative humidity at
 351 the initial stage of homogeneous mixing before droplets start evaporating (Fig. 1b2). Figure 3h
 352 presents comparisons of modeled $T(\mu)$ and those calculated from Eqs.(6a,b) and (C4). The
 353 independence of $q(\mu)$, $RH(\mu)$ and $T(\mu)$ on type of mixing (Fig.4a,g,h) is the consequence of the
 354 mass and energy conservation, which are not contingent on type of mixing.

355

356 3.2 Effect of humidity of entrained air

357 The diagrams in Fig. 5a-c show the dependences of normalized β , q and D_v vs. N/N_0 calculated from numerical simulations and analytical equations from Sect. 2. The calculations were
 358 performed for different humidity of the entrained air RH_2 . As seen from Fig. 5a-c, the normalized
 359 dependences for homogeneous mixing $q(N)$, $\beta(N)$ and $D_v(N)$ tend to approach the line of extreme
 360 inhomogeneous mixing when relative humidity RH_2 approaches to 1. This is consistent with the
 361 degenerate case, when $\xi \rightarrow 0$ (Sect.2.7). In this case droplets behave as a passive admixture, and they
 362 do not interact with the environment.
 363

364

365 **3.3 Effect of liquid water mixing ratio**

366 Figure 5d-f demonstrate the sensitivity of $q(N)$, $\beta(N)$ and $D_v(N)$ to liquid water mixing ratio
 367 q_1 . It is seen, that the increase of q_1 results in $q(N)$, $\beta(N)$ and $D_v(N)$ (calculated for homogeneous
 368 mixing) approaching towards $q(N)$, $\beta(N)$ and $D_v(N)$ for the inhomogeneous mixing. In other words,
 369 the sensitivity of the microphysical parameters to the type of mixing increases with the decrease of
 370 q_1 . From a practical viewpoint it means, that from in-situ observations the difference between
 371 homogeneous and inhomogeneous mixing is anticipated to be more pronounced for the cases with a
 372 relatively low liquid water mixing ratio (e.g. $q_1 < 1\text{g/kg}$). Such behaviour is consistent with the
 373 consideration in Sect. 2.7.
 374

374

375 **3.4 Effect of temperature, case $T_1 = T_2$**

376 Figure 5g-j shows the effect of temperature on the normalized $q(N)$, $\beta(N)$ and $D_v(N)$ for $T_1 =$
 377 T_2 . Figure 5g-j indicate that the difference between the moments becomes most pronounced at warm
 378 temperatures, whereas at cold temperatures (e.g. $T = -30^\circ\text{C}$), $q(N)$, $\beta(N)$ and $D_v(N)$ for
 379 homogeneous mixing are approaching those for the extreme inhomogeneous mixing limit.

380 Such behavior is explained by the fact that liquid water deficit δq_m decreases with decreasing
 381 temperature (appendix A, Fig. A1). At low temperatures ($T = -30^\circ\text{C}$) the amount of evaporated water
 382 δq_m is so small, that homogeneous mixing with dry out-of-cloud air will have approximately the
 383 same effect as mixing with saturated air (i.e. degenerate case, Sect. 2.7).

384 Overall, as follows from Fig.5 the results the analytical predictions (Sect. 2) turned out to be in
 385 a good agreement with numerical simulations.
 386

386

387 **3.5 Effect of temperature, case $T_1 \neq T_2$**

388 Isobaric mixing of two nearly saturated volumes with $T_1 \neq T_2$ may result in supersaturated
389 environment (e.g. Rogers, 1976; Bohren and Albrecht, 1998). Mixing resulting in supersaturation is
390 different in principle from the mixing with evaporating droplets. In this case the meaning of
391 homogeneous and inhomogeneous mixing becomes ambiguous. Formation of supersaturation leads
392 to different dependences between $N\bar{D}$, β , q , \bar{D} and N as compared to those shown in Figs. 3–4, when
393 $T_1 = T_2$.

394 Figure 6 presents a set of diagrams similar to those in Fig.4, but calculated for the cases when
395 $T_1 \leq T_2$. It turns out that for the case of extreme inhomogeneous mixing the temperature difference
396 between T_1 and T_2 breaks down linear dependences of the microphysical moments (e.g. $N\bar{D}$, β , q
397 Fig. 6a,c,d) vs. μ .

398 Figure 7 presents the effect of the temperature difference ΔT on the normalized dependences
399 $q(N)$, $\beta(N)$ and $D_v(N)$. In clouds, high supersaturation resulting from isobaric mixing may lead to
400 activation of interstitial CCN, which may increase N and decrease D_v (Korolev and Isaac, 2000).
401 However, no activation of new droplets during isobaric mixing was allowed in this study. For the
402 cases when $RH_{m0} > 1$ (Fig. 7, *AB* on line 1) the condensed water was uniformly distributed between
403 available droplets. Therefore, $q(N)$, $\beta(N)$ and $D_v(N)$ calculated for homogeneous and
404 extremely extreme inhomogeneous mixing coincide with each other on this interval.

405 Numerical simulations also showed, that the effect of temperature on mixing is more pronounced
406 for the cases, when the cloud temperature is warmer than that of the entrained air, i.e. $T_1 > T_2$, as
407 compared to the cases with $T_1 < T_2$.

408

409 **4. Progressive mixing**

410 **4.1 Effect on microphysical parameters**

411 In the previous sections the mixing was considered as a single event, i.e. μ fraction of the cloudy
412 air mixed up with $(1 - \mu)$ fraction of entrained dry air. Such mixing will be referred to as “primary”
413 mixing. Primary mixing results in an ensemble of elementary volumes characterized by a set of
414 microphysical and state parameters i.e. $\bar{D}_v(\mu)$, $N(\mu)$, $RH(\mu)$, $T(\mu)$, etc. Each of these parameters
415 has a functional dependence on μ , and what is important, these parameters have functional
416 relationships between each other.

417 In reality mixing is a continuous process. It does not stop after the primary mixing. The
418 elementary volumes formed after primary mixing continue to progressively mix with each other.

419 The second stage of mixing will result in an ensemble of elementary volumes characterized by
420 a set of parameters $D_v^{(2)}$, $N^{(2)}$, $RH^{(2)}$, $T^{(2)}$, etc. Here the superscript ⁽²⁾ indicates the stage of mixing.
421 After the second stage the mixed volumes undergo subsequent stages of mixing.

422 The idealised conceptual diagram of the progressive mixing is shown in Fig. 8. Each stage of
423 mixing results in an ensemble of elementary parcels formed for different $\mu_j^{(n)}$. The elementary
424 parcels continue mixing with each other and cloud environment during the subsequent mixing stages.

425 As mentioned in Sect. 2.1, the actual process of mixing is indeed much more complex than the
426 sequence of discrete events portrayed in Fig.8. However, as it will be shown below, this simplified
427 consideration of allows establishing main features of evolution of relationships between the
428 microphysical moments affected by mixing. The obtained results facilitates facilitate identification
429 of type of mixing from in-situ measurements.

430 Progressive homogeneous mixing was simulated with the help of a numerical model, where
431 parcels were randomly mixed with each other and with the cloud environment. The mixing fraction
432 μ was also set to be random during each mixing event. Models of stochastic mixing have been used
433 in a number of studies (e.g. Krueger et al., 1997; Su et al., 1998; Burnet and Brenguier, 2007). In the
434 present work the analysis of progressive mixing is expanded to examine its effect on the relationship
435 between moments of the droplet size distribution.

436 The results of the progressive homogeneous mixing for the first four stages are presented in Fig.
437 9. As seen from Fig. 9 the functional relationship between the pairs of microphysical and state
438 parameters exists only for the primary stage. For higher mixing stages these functional relationships
439 break down. Thus, cloud volumes with the same $N^{(2)}$ may have different $D_v^{(2)}$. Figure 9 also shows
440 that the regions of scattering of $q(N)$, $\beta(N)$ and $D_v(N)$ for stages 2, 3 and 4 are limited from above
441 by the inhomogeneous mixing (red dashed lines) and from below by primary homogeneous mixing
442 (red solid lines).

443 Figure 10 presents a conceptual $N - q$ diagram explaining breaking the functional relationships
444 during progressive homogeneous mixing. After the first stage of mixing the $N - q$ points will be
445 scattered along the line OB and point C . The line OB corresponds to the ensemble of points with
446 $RH = 1$. Therefore, result of mixing between two saturated volumes randomly selected on AB , will
447 remain on the same line. Point C corresponds to the ensemble of points with $N = 0$, $RH_2 \leq$
448 $RH_C(\mu^{(1)}) \leq 1$, where $0 \leq \mu^{(1)} < \mu_{cr}$. Therefore, mixing between point A (Fig.10) and point C ,

449 when $RH = 1$ will result in scattering along the line AC (degenerate case). Points resulted from
 450 mixing between A ($RH = 1$) and point C , when $RH_2 \leq RH_C < 1$, will scattered over the ensemble
 451 of dashed lines shown in Fig.10. These lines will fill the sector CAB . Random mixing between points
 452 on the line OB and C , will eventually fill the entire sector COB . The same consideration can be
 453 applied to progressive mixing between other moments.

454 During the progressive mixing $N^{(n)}$, $\beta^{(n)}$, $q^{(n)}$ and $D_v^{(n)}$ formed in the elementary parcels tend
 455 to approach those in the undiluted cloud, i.e. N_1 , β_1 , q_1 and D_{v1} . This process can be considered as
 456 a surrogate to the diffusion process between the cloud and sub-saturated out-of-cloud environment.
 457 The convergence of $\beta^{(n)}$, $q^{(n)}$ and $D_v^{(n)}$ during the progressive mixing can be seen in Fig. 9, where
 458 the scattering of normalized $q^{(n)}(N)$, $\beta^{(n)}(N)$ and $D_v^{(n)}(N)$ becomes denser towards the top-right
 459 corner (1,1) with the increase of the stage of mixing.

460 It is worth noting that progressive mixing with the dry air only does not break the functional
 461 relationships between the moments. This case is equivalent to detrainment of cloudy environment
 462 into dry air. It can be shown that Eq.(14) remain valid at any stage of progressive homogeneous
 463 mixing with dry air only, i.e. $N_j/N_1 = \mu^{(1)} \dots \mu^{(j-1)} \mu^{(j)} N_j/N_1 = \mu^{(1)} \dots \mu^{(n-1)} \mu^{(n)}$ where $\mu^{(j)}$
 464 is the mixing fraction at the j -th stage of mixing. Eqs. (15)-(24) also remain valid for the progressive
 465 mixing with the dry air only.

466 As follows from Eq. (9) for the case of extreme inhomogeneous mixing the progressive mixing
 467 does not affect the functional relations between $N^{(n)}$, $\beta^{(n)}$, $q^{(n)}$ and $D_v^{(n)}$ and other microphysical
 468 parameters. These relations remain the same regardless of the actual stage of mixing. This is one of
 469 the fundamental differences between homogeneous and **extreme** inhomogeneous mixing, which can
 470 be used for identification of type of mixing from in-situ measurements.

471
 472 **4.2 Effect on droplet size distributions**

473 Figure 11 shows modeled droplet size distributions averaged over the ensembles of elementary
 474 volumes corresponding to the first four stages of homogeneous mixing. As seen from Fig. 11a-d for
 475 the case with $T_1 = T_2$ the droplet size distributions are broadened towards small sizes. Depending on
 476 the stage of mixing and mixing fraction μ the size distributions formed in each elementary volume
 477 may be unimodal or multimodal. However, due to the random nature of the modal sizes formed
 478 during mixing, the average size distributions become smooth and unimodal (Fig.11a-d).

479 Broadening of droplet size distributions towards small sizes during homogeneous mixing is well
 480 known and it was demonstrated in a number of studies (e.g. Baker and Latham, 1982; Jensen and
 481 Baker, 1989; Jeffery, 2007; Kumar et al., 2013). However, if mixing results in supersaturation
 482 (section 3.4), then the droplet size distribution may broaden towards larger sizes (Fig. 11e–h). For
 483 this to occur, both the temperature difference between the cloud and the environment $[T_1 - T_2]$ and
 484 the relative humidity of the environment RH_2 must be sufficiently large. Such conditions are
 485 inherently unstable, however, this might occur in regions that have been moistened through prior
 486 cloud detrainment. Thus homogeneous mixing may result in broadening of droplet size distributions
 487 towards either smaller or larger sizes (Fig.11).

488 These results were obtained in the frame of the formalism of homogeneous and inhomogeneous
 489 mixing. The following two works in this series (Pinsky et al., 2015a,2016a, b) will discuss the
 490 broadening of polydisperse and monodisperse $f(D)$ during both homogeneous and inhomogeneous
 491 mixing in greater details.

492

493 **5 Identification of type of mixing from in-situ observations**

494 The purpose of this section is to attempt identifying type of mixing based on examining
 495 relationships between basic microphysical parameters N , β , LWC , D_v measured from in-situ.

496 **5.1 Expected relationships between the moments**

497 Prior proceeding with the analysis of in-situ data we summarize the results of the previous
 498 consideration on how homogeneous and extreme inhomogeneous mixing is expected to manifest
 499 itself in relationships between basic microphysical parameters, such as N , β , q and D_v .

500 For extreme inhomogeneous mixing the relationship between the pairs of N , β and q are
 501 determined by linear dependences $M_n = \alpha_{nm} M_m$ (Eq. 10) at any stage of mixing. As follows
 502 from Eq. (11) the slopes α_{nm} for $q(N)$, $\beta(N)$ and $q(\beta)$ are equal to the ratios q_1/N_1 , β_1/N_1 ,
 503 and q_1/β_1 , respectively, where N_1 , β_1 and q_1 correspond to undiluted adiabatic values. The values
 504 of N_1 , β_1 and q_1 may vary depending on the location inside the cloud and environmental conditions
 505 at the cloud base. Thus, the adiabatic value of q_1 is a function of elevation above the cloud base ΔZ ,
 506 whereas N_1 depends on the vertical velocity at the cloud base u_z and the aerosol load. Therefore, the
 507 scattering of $q - N$ points will be aligned along an ensemble of different lines determined by q_1/N_1 ,
 508 which are specific to different cloud volumes. The conceptual diagram of the scattering of $q - N$

509 measurements in a cloud with extreme inhomogeneous mixing is shown in Fig. 12a. The scatter
510 diagrams for other moments (e.g. $q - \beta$, $N - \beta$) will have the similar patterns as that in Fig. 12a.

511 For the case of homogeneous mixing the functional relationship between the pairs of N , β , q
512 and D_v are disrupted by a progressive mixing. As shown in Sect. 4.1 the ensemble of points of N , β
513 and q will be scattered within a sector, which is limited by lines determined by Eq. (11) (extreme
514 inhomogeneous mixing) and Eqs. (15)-(17) (primary homogeneous), respectively (Fig. 9). What is
515 important, is that the top of the sectors for $q(N)$ and $\beta(N)$ correspond to points $[N_1, q_1]$ and $[N_1, \beta_1]$,
516 respectively. Since N_1 , β_1 and q_1 may vary within the same cloud, it is anticipated that the N , β and
517 q measurements will be scattered within an ensemble of sectors as shown in Fig. 12b.

518 It is important to note that that during homogeneous mixing prior reaching equilibrium,
519 functional relationships between the microphysical moments do not exist either. After the instant
520 mixing of cloud fraction μ with entrained air (Fig. 1b(2)), $q_{m0} = \mu q_0$ and $N_{m0} = \mu N_0$. This state
521 corresponds to point D in Fig.10. After that droplets start evaporating until liquid mixing ratio
522 reaches point A (Fig.10), which corresponds to the equilibrium state ($RH = 1$). Therefore, during
523 evaporation time $q - N$ points will be scattered along the line AD . Since, point D can be located
524 anywhere on OC , the ensemble of $q - N$ points corresponding to non-equilibrium state will fill the
525 COB area.

526 Thus, the absence of the functional relationships between the moments during homogeneous
527 mixing may occur both during progressive mixing and during primary mixing prior reaching the
528 equilibrium state. The evaporation time required to reach equilibrium during homogeneous mixing
529 is discussed in details in Pinsky et al. (2015b,2016b), and it is usually limited by few tens of seconds.
530 However, progressive mixing is not limited in time. Therefore, it is very likely that no functional
531 relationship between microphysical parameters will be observed during in-situ measurements.

532 Fig.12 demonstrated a fundamental difference in scattering of $q - N$ for homogeneous and
533 extreme inhomogeneous mixing, which will be used to facilitate identification of type of mixing in
534 the following section.

535

536 **5.2 Results of observations**

537 The measurements were obtained on the University of Wyoming King Air aircraft during the
538 COPE-MED project in South-Western part of UK during July-August 2013 (Leon et al., 2016). The
539 UW King Air was equipped with a suite of microphysical instruments, including a DMT Cloud

540 Droplet probe (CDP), designed for measurements of droplet sizes and their concentrations in the
541 nominal size ranges 1–50 μm .

542 Figure 13 shows a time series of droplet concentration, extinction coefficient, liquid water
543 content and mean volume droplet diameter measured by the CDP during transit through a convective
544 cell on 18 July 2013. The CDP data were sampled at 10Hz, which corresponds to approximately 10m
545 spatial averaging. Visual examination of the spatial changes of N , β and LWC shows strong
546 correlation. The amplitude of changes of these parameters reaches nearly one hundred percent with
547 respect to their maximum. Contrary to that, the spatial variations of \bar{D} and D_v are quite conservative
548 and their values remain nearly constant. With the exception of two cloud holes between 13:50:42
549 and 13:50:44, the amplitude of fluctuations of D_v does not exceed 8% with standard deviation of
550 2.2%.

551 Figure 14 shows scatter diagrams of $LWC(N)$, $\beta(N)$, $LWC(\beta)$ and $D_v(N)$ measured by the CDP
552 during seven consecutive penetrations of the same convective cell extended over a period of
553 approximately 19 min. One of these penetrations is shown in Fig. 13. The measurements were
554 conducted at $H = 5500\text{m}$ and $T = -12^\circ\text{C}$. The relative humidity of the ambient air was approximately
555 20 %. At the beginning of the sampling no precipitation size particles were observed in the cloud.
556 However, by the end of the sampling period some raindrops and ice crystals were present in the
557 cloud. Despite the presence of some precipitation size particles, the scatter diagrams in Fig. 14a, b
558 and d demonstrate high correlation between pairs N , β and LWC . The mean volume diameter in Fig.
559 14c shows very little changes from 19 to 17 μm , when concentration changes from 1100 to 500 cm^{-3} .
560 However, for $N < 200 \text{ cm}^{-3}$, the volume diameter decreases to 12–15 μm .

561 Red lines in Fig. 14 indicate $q(N)$, $\beta(N)$, $LWC(\beta)$ and $D_v(N)$ calculated for the 1st stage of
562 homogeneous mixing. The calculations were performed for a monodisperse $f(D)$ with $D_1=18.5\mu\text{m}$,
563 $N_1 = 1100 \text{ cm}^{-3}$, and state parameters as during the measurements. Comparisons of dependences
564 $q(N)$, $\beta(N)$, $LWC(\beta)$ and $D_v(N)$ based on in-situ measurements with those obtained from numerical
565 simulations of homogeneous mixing show minor difference for high concentrations $700 \text{ cm}^{-3} < N <$
566 1100 cm^{-3} (Fig. 14a–c). Simulation also shows that for this specific case the difference between
567 homogeneous and inhomogeneous mixing does not exceed 10% when $700 \text{ cm}^{-3} < N < 1100 \text{ cm}^{-3}$.
568 Such difference remains within the errors of measurements. Therefore, in this specific cloud for the
569 regions with $N > 700 \text{ cm}^{-3}$ the type of mixing cannot be unambiguously identified from the analysis
570 of the dependences $LWC(N)$, $\beta(N)$, $LWC(\beta)$ and $D_v(N)$. This is consistent with the assessment of

571 feasibility of segregation of homogeneous and inhomogeneous mixing in Fig.3 (dashed line). Since
572 for homogeneous mixing $N \propto \mu$, then $= \frac{N}{N_1}$ (Eq.(14)), then assuming $N_1 = 1100 \text{ cm}^{-3}$, Fig.3 suggests
573 good separation of the moments for $N \gg 700 \text{ cm}^{-3}$.

574 For the regions with $N < 500 \text{ cm}^{-3}$ the deviation between homogeneous mixing simulations and
575 in-situ measurements in Fig.14 becomes well pronounced, and it extends beyond possible errors of
576 measurements. This suggests that the mixing ~~is~~ in these regions is dominated by the extreme
577 inhomogeneous type.

578 Figure 15 shows the same type of diagrams as in Fig. 14, which were measured during 45
579 consecutive traverses through an ensemble of deep convective cells. The sampling altitude varied in
580 the range $3000 \text{ m} < H < 4500 \text{ m}$, temperature $-11^\circ \text{C} < T < 0^\circ \text{C}$, relative humidity in the vicinity of
581 clouds $15\% < \text{RH} < 65\%$. The cloud measurements were extended over a period of 2 h 13 m, which
582 is suggestive that the convective cells were sampled at different stages of their lifetime. At the
583 sampling level the concentration of raindrops varied from zero to few per liter, and their diameter
584 did not exceed 2mm.

585 What is interesting that the scattering of ~~the measurements~~ $LWC(N)$, $\beta(N)$ and $LWC(\beta)$ (Fig.
586 15a, b and d) is limited by the sector, which originates from the zero point as in Fig.12a. Analysis of
587 the measurements showed that the data points $LWC(N)$, $\beta(N)$, $LWC(\beta)$ in each individual cloud
588 traverse are well aligned along the lines with different slopes (e.g. Fig.14). After averaging over the
589 ensemble of clouds, the area of the scattered points turned out to be located inside a sector limited
590 by the lines with smallest and largest slopes.

591 Comparisons of the scatterdiagrams $LWC(N)$, $\beta(N)$ and $LWC(\beta)$ in Figs.14 and 15 with the
592 conceptual diagrams in Fig.12 unambiguously suggest that interaction between cloud and
593 environment in the studied clouds was dominated by inhomogeneous mixing. It should be
594 emphasized that analysis of a stand alone mixing diagram $N - D_v$ would not allow unambiguously
595 draw such conclusion.

596

597 6. Discussion

598 One of the assumptions in most past studies is that for a sequence of the cloud samples collected
599 along the flight path, the adiabatic values of N_1 , q_1 , β_1 , D_1 and environmental parameters e_2 and T_2
600 remain the same. In fact these parameters may vary both within the same cloud or sequence of
601 samples clouds, and the amplitude of their variations depends on microphysical and

602 thermodynamical properties inside and outside the cloud environment. This variation will result in
603 an ensemble of relationships $M_n = F_{nk}(M_k)$, and enhance scattering of the data points. In such cases
604 identification of the type of mixing based on the $N - D_v$ diagram may result in confusion between
605 homogeneous and inhomogeneous mixing. As demonstrated in Sect. 5, consideration of $N - q$ and
606 $N - \beta$ diagrams may provide a better identification type of mixing.

607 Strictly speaking the identification of type of mixing from particle probe measurements as it was
608 performed in Sect. 5 is incomplete. It allows establishing correlation between microphysical
609 moments and makes a formal conclusion about the mixing type, however it does not allow judgement
610 about stage of mixing (i.e. whether mixing is complete by reaching equilibrium). In most previous
611 studies, including this one, identification of type of mixing was based on the assumption that the
612 sampled cloud volume is in equilibrium state ($RH = 1$), and that it reached the final stage of mixing
613 (Fig.1 a2, a3, b3). It is possible that at the moment of measurement the process of mixing is not
614 complete and the droplet free filaments remained undersaturated (Fig.1 a1, b1, b2). In this case the
615 relationship between different moments may be well described as $M_n = \alpha_{nk}M_{nk}$ and the mixing be
616 confused with inhomogeneous mixing.

617 In order to identify stage of mixing, high frequency collocated measurements of temperature and
618 humidity are required. Unfortunately, current technology does not allow such measurements yet.

619 ~~Identification of type of mixing from in situ observations is based on examination of~~
620 ~~relationships between moments of the size distributions measured along the flight path.~~ The basic
621 assumption underlying ~~this~~the analysis of relationships between moments is that the cloud
622 environment is not affected by other non-adiabatic processes.

623 Thus, collision-coalescence, riming or Wegener-Bergeron-Findeisen processes may change the
624 droplet number concentration and liquid water content, and therefore, affect the relationship between
625 the moments. Activation of interstitial CCN will result in breaking correlation between the moments
626 due to formation of large concentration of droplets. Broad size distributions may also hinder
627 identification of type of mixing due to partial evaporation of small droplets (Pinsky et al.
628 2015a,2016a)

629 It is anticipated that most suitable candidates to study mixing-entrainment process are non-
630 precipitating convective clouds and stratocumulus clouds with relatively narrow droplet size
631 distributions.

632 Another limiting factor is that the above consideration did not account for the effect of changing
633 relative humidity in a vertically ascending parcel. Thus in droplet free entrained air RH increases
634 approximately 10% for $\Delta z = 200\text{m}$ at $T = 0\text{ }^\circ\text{C}$. After reaching saturation the mixing turns into a
635 degenerate case, which will appear as extreme inhomogeneous mixing. Joint effects of evaporating
636 droplets and an increase in RH during the vertical ascent may facilitate reaching saturation state. This
637 case may also be relevant to the convective cloud described in Sect.5.2.

638

639

640

641 7. Conclusions

642 This study analyzes dependences of different moments of $f(D)$ in the frame of formalism of
643 homogeneous and ~~extremely~~ extreme inhomogeneous mixing. The analysis was performed for the
644 final stage of mixing based on the mass and energy conservation consideration. The following results
645 were obtained in the frame of this study:

646 1. Simple analytical relationships between the main microphysical moments were obtained for
647 the final state homogenous and extreme inhomogeneous mixing.

648 2. It was shown that the functional relationships between the moments exist only for the first
649 stage of homogeneous mixing, when equilibrium is reached. Subsequent progressive homogeneous
650 mixing breaks the functional relationship between the moments.

651 3. It was demonstrated that consideration of scattering $N - LWC$, $N - \beta$ diagrams facilitates
652 identification of type of mixing from in-situ measurements. For extreme inhomogeneous mixing the
653 scattering of the data points $N - LWC$, $N - \beta$ will be limited by a sector originating at zero point
654 (Fig.12a). However, for homogeneous mixing the scattering data points will be limited by a sector
655 originating at (N_1, LWC_1) and (N_1, β_1) (Fig.12b). Utilizing a stand-alone conventional $N - D_v$
656 mixing diagram may not provide unambiguous answer about type of mixing.

657 4. The developed approach was applied to a set of in-situ measurements collected in convective
658 clouds. The analysis of the dependences between N , β , LWC and D_v suggests that the interaction
659 between entrained and cloudy environments for the studied clouds was dominated by
660 inhomogeneous mixing.

661 The present study considers relationships between different moments of $f(D)$ for the final stage
662 of mixing. The following two works Pinsky et al. (2015a, 2016a, b) in this series provide a detailed

663 analysis of time dependences of droplet size distributions and its moments during homogeneous and
 664 inhomogeneous mixing.

665
 666 *Acknowledgement.* The authors appreciate two anonymous reviewers for their comments. Alexei
 667 Korolev work was supported by Environment Canada and Transport Canada. The COPE-MED
 668 project was funded by National Science Foundation grant AGS-1230292 and AGS-1230203. The
 669 contribution of Mark Pinsky and Alex Khain was supported by the Israel Science Foundation (grant
 670 1393/14), the Office of Science (BER), US Department of Energy Award DE-SC0006788 and the
 671 Binational US-Israel Science foundation (grant 2010446).

672
 673 **Appendix A: Liquid water deficit**

674 The objective of this section is to find the amount of liquid water, which is required to be
 675 evaporated in order to saturate the parcel formed after mixing. Assume that q_{v1} , q_{v2} are the mixing
 676 vapor ratios in the cloudy and entrained parcels, respectively, and T_1 , T_2 are their respective initial
 677 temperatures. First, we find the saturation ratio S_{m0} formed after instant mixing of the cloud and
 678 entrained before the cloud droplets start evaporating.

679 The vapor mixing ratio q_{vm} formed in the mixed volume will be
 680
$$q_{vm} = \mu q_{v1} + (1 - \mu) q_{v2} \quad (A1)$$

681 The vapor pressure e_m in the mixed volume can be derived from Eq. (A1) by substituting

682
$$q_v = \frac{e}{p - e} \frac{R_a}{R_v}, \text{ i.e.}$$

$$e_m = p \frac{\mu + \frac{e_2(p - e_1)}{p(e_1 - e_2)}}{\mu + \frac{(p - e_1)}{(e_1 - e_2)}} \quad (A2)$$

684 The temperature of the mixed volume T_{m0} can be found from the energy conservation law
 685
$$\mu(q_{v1}c_{pv} + c_{pa})(T_1 - T_{m0}) = (1 - \mu)(q_{v2}c_{pv} + c_{pa})(T_{m0} - T_2) \quad (A3)$$

686 here c_{pv} , c_{pa} are the specific heat capacitance of water vapor and dry air at constant pressure,
 687 respectively, ~~T_1 , T_2 are the initial temperatures in the first and second parcels before mixing.~~
 688 Substituting q_{v1} , q_{v2} yields the temperature in the mixed volume

689
$$T_{m0} = \frac{\mu T_1 + \alpha(1-\mu)T_2}{\mu + \alpha(1-\mu)} \quad (\text{A4})$$

690 here

691
$$\alpha = \frac{1 + \frac{c_{pv}R_a e_2}{c_{pa}R_v(p-e_2)}}{1 + \frac{c_{pv}R_a e_1}{c_{pa}R_v(p-e_1)}} \quad (\text{A5})$$

692 With a good accuracy $\alpha \cong 1$. The resulting relative humidity after mixing the two volumes will
693 be

694
$$RH_{m0} = \frac{e_{m0}}{e_s(T_{m0})} \quad (\text{A6})$$

695 where $e_s(T_{m0})$ is the saturated vapor pressure at temperature T_{m0} .

696 The process of evaporation is accompanied by changing humidity and temperature due to latent
697 heat of vaporization. This process is described by the Eq. (C2) in Korolev and Mazin (2003).
698 Assuming the process to be isobaric (i.e. vertical velocity $u_z = 0$) and absence of ice ($dq_i = 0$), Eq.
699 (C2) (Korolev and Mazin, 2003) yields

700
$$\frac{dS}{S+1} = \left(\frac{1}{S+1} \frac{pR_v}{e_s R_a} + \frac{L^2}{c_{pa}R_v T^2} \right) dq \quad (\text{A7})$$

701 Integrating Eq. (A7) from initial S_{m0} to saturation state, when $S = 0$, and taking into account
702 that $RH = S + 1$, gives

703
$$\delta q_m = -b \ln \left(\frac{1 + aRH_{m0}}{1 + a} \right) \quad (\text{A8})$$

704 the mixing ratio of liquid water required to evaporate in order to saturate 1kg of the cloud volume
705 formed after mixing with the entrained air, but before droplet start evaporating. Here $a = \frac{E_s R_a L^2}{p c_p R_v^2 T_{m0}^2}$,

706
$$b = \frac{c_p R_v T_{m0}^2}{L^2}.$$

707 Since $\left| \frac{a(RH_{m0}-1)}{1+a} \right|$ Rewriting the right side of Eq.(A8) as $-b \ln \left(1 + \frac{a(RH_{m0}-1)}{1+a} \right)$, and taking into
708 account that $\left| \frac{a(RH_{m0}-1)}{1+a} \right| < 1$, Eq.(A8) can be simplified as

709
$$\delta q_m = ab \frac{1 - RH_{m0}}{1 + a} = -\frac{S_{m0}}{A_2} \quad (\text{A9})$$

710 where $A_2 = \frac{ab}{1+a}$. The analysis of Eqs. (A8)-(A9) shows that for wide range of temperatures $-30^\circ\text{C} <$
 711 $T < 30^\circ\text{C}$, both equations hold with high accuracy as long as the temperatures of the sub-saturated
 712 and cloud parcels $|T_1 - T_2| < 10^\circ\text{C}$.

713 Figure A1 shows comparisons of modeled δq_m and that calculated from Eqs. (A8) and (A9) for
 714 three different temperatures. The model solved a system of differential equation with incremental
 715 evaporation of liquid water until saturation is reached. As seen from Fig. A1 the agreement between
 716 modeled δq_m and that calculated from Eqs. (A8)-(A9) is quite good and does not exceed few
 717 percent at $RH_{m0} = 0.5$. This discrepancy results from assumption that e_s and T are constant in
 718 Eqs.(A8)-(A9).

719

720 **Appendix B: Liquid water deficit when $T_1 = T_2$**

721 Eq.(A2) by assuming that $p \gg e_1$ and $p \gg e_2$ can be simplified as

$$722 \quad e_{m0} = \mu e_1 + (1 - \mu)e_2 \quad (\text{B2})$$

723 As follows from Eq.(A4) for the case $T_1 = T_2$ with high accuracy $T_{m0} = T_1 = T_2$. Therefore,
 724 $e_s(T_{m0}) = e_s(T_1) = e_s(T_2)$. Dividing Eq.(B1) by e_s yields

$$725 \quad RH_{m0} = \mu RH_1 + (1 - \mu)RH_2 \quad (\text{B3})$$

726 In most liquid clouds $RH_1 = 1$ (Korolev and Mazin 2003). Therefore, Eq.B2 turns into

$$727 \quad RH_{m0} = \mu + (1 - \mu)RH_2 \quad (\text{B4})$$

728 Substituting Eq.(B4) in Eq.(B1) yields

$$729 \quad \delta q_m = -b \ln \left(1 + \frac{a(1 - \mu)(RH_2 - 1)}{1 + a} \right) \quad (\text{B5})$$

730 The expression under logarithm can be presented as the first two terms of the series expansion

731 of $\left(1 + \frac{a(RH_2 - 1)}{1 + a} \right)^{(1 - \mu)} \left(1 + \frac{a(RH_2 - 1)}{1 + a} \right)^{(1 - \mu)}$. Substituting this expression into Eq.(B5), gives

$$732 \quad \delta q_m = (1 - \mu)\delta q^* \quad (\text{B6})$$

733 where

$$734 \quad \delta q^* = -b \ln \left(\frac{1 + aRH_2}{1 + a} \right) \quad (\text{B7})$$

735 is the mixing ratio of liquid water required to saturate 1 kg of the entrained dry volume.

736

737 **Appendix C: Temperature in the mixing volume**

738 The energy conservation for evaporating droplets can be written as

739
$$(T - T_{m0})(1 + q_{vm})c_{pm} + (1 - \mu)\delta q^* L = 0 \quad (C1)$$

740 here c_{pm} is the specific heat capacity of the moist air

741
$$c_{pm} = \frac{c_{pa} + q_{vm}c_{pv}}{1 + q_{vm}} \quad (C2)$$

742 Since $q_{vm} \ll 1$ and, $c_{pa} \cong c_{pm}$ Eq.(C1) may be simplified, so that the final temperature after mixing

743
$$T = T_{m0} - \frac{(1 - \mu)\delta q^* L}{c_{pa}} \quad (C3)$$

744 For the case when $T_1 \neq T_2$ Eq. (C3) should be replaced by

745
$$T = T_{m0} - \frac{\delta q_m L}{c_{pa}} \quad (C4)$$

746 Eqs. (C3) and (C4) are valid for the mixing fraction $\mu > \mu_{cr}$. For $\mu \leq \mu_{cr}$ all entrained liquid
747 water μq_0 evaporates, and the final temperature will be

748
$$T = T_{m0} - \frac{\mu q_0 L}{c_{pa}} \quad (C5)$$

749

750 **References**

751 Andrejczuk M., Grabowski, W. W., Malinowski, S. P., and Smolarkiewicz, P. K.: Numerical
752 simulation of cloud-clear air interfacial mixing: homogeneous vs. inhomogeneous mixing., J.
753 Atmos. Sci., 66, 2493-2500, 2009.

754 Baker, M. B. and Latham, J.: The evolution of droplet spectra and the rate of production of embryonic
755 raindrops in small cumulus clouds, J. Atmos. Sci., 36, 1612–1615, 1979.

756 Baker, M. B. and Latham, J.: A diffusive model of the turbulent mixing of dry and cloudy air, Q. J.
757 R. Met. Soc., 108, 871–898, 1982.

758 Baker, M. B., Corbin, R. G., and Latham, J.: The influence of entrainment on the evolution of cloud droplet
759 spectra: I. A model of inhomogeneous mixing, Q. J. Roy. Meteor. Soc., 106, 581–598, 1980.

760 Beals, M.J., and Fugal, J.P., Shaw, R.A., Lu, J., Spuler, S.M., Stith, J.L.: Holographic measurements
761 of inhomogeneous cloud mixing at the centimeter scale. Science, 350, 87-90, 2015

Formatted: Font: 11 pt

762 Bohren, C. F. and Albrecht, C. H.: Atmospheric Thermodynamics, Oxford University Press, New
763 York, 402 pp., 1998.

764 Bower, K. N. and Choullarton, T. W.: The effects of entrainment on the growth of droplets in
765 continental cumulus clouds, *Q. J. Roy. Meteor. Soc.*, 114, 1411–1434, 1988.

766 Broadwell, J. E., and R. E. Breidenthal: A simple model of mixing and chemical reaction in a
767 turbulent shear layer. *J. Fluid Mech.*, 125, 397–410, 1982

768 Burnet, F. and Brenguier, J. L.: Observational study of the entrainment-mixing process in warm
769 convective clouds, *J. Atmos. Sci.*, 64, 1995–2011, 2007.

770 Devenish, B. J., Bartello, P., Brenguier, J.-L., Collins, L. R., Grabowski, W. W., Ijzermans, R. H.
771 A., Malinowski, S. P., Reeks, M.W., Vassilicos, J. C., Wang, L- P., and Warhaft, Z.: Droplet growth
772 in warm turbulent clouds, *Q. J. Roy. Meteor. Soc.*, 138, 1401–1429, 2012.

773 ~~Dimotakis, P. E.: Turbulent mixing, *Annu. Rev. Fluid Mech.*, 37, 329–356, 2005.~~

774 Gerber, H., Frick, G., Jensen, J. B., and Hudson, J. G.: Entrainment, mixing, and microphysics in
775 trade-wind cumulus, *J. Meteorol. Soc. Jpn.*, 86, 87–106, 2008.

776 Hill, T. A. and Choullarton, T. W.: An airborne study of the microphysical structure of cumulus clouds,
777 *Q. J. Roy. Meteor. Soc.*, 111, 517–544, 1985.

778 ~~Jeffery, C. A.: Inhomogeneous cloud evaporation, invariance, and Damköhler number, *J. Geophys.*
779 *Res.*, 112, D24S21, doi:10.1029/2007JD008789, 2007.~~

780 Jarecka, D., Grabowski, W. W., Morrison, H., Pawlowska, H.: Homogeneity of the Subgrid-Scale
781 Turbulent Mixing in Large-Eddy Simulation of Shallow Convection. *J. Atmos. Sci.* 70, 2751-
782 2767, 2013

783 ~~Jeffery, C. A.: Inhomogeneous cloud evaporation, invariance, and Damköhler number, *J. Geophys.*
784 *Res.*, 112, D24S21, doi:10.1029/2007JD008789, 2007.~~

785 Jensen, J. and Baker, M.: A simple model of droplet spectra evolution during turbulent mixing, *J.*
786 *Atmos. Sci.*, 46, 2812–2829, 1989.

787 Korolev A. V.: The influence of supersaturation fluctuations on droplet spectra formation. *Journal*
788 *of the Atmospheric Sciences*, 52, 3620-3634, 1995.

789 Korolev, A. V. and Isaac, G. A.: Drop growth due to high supersaturation caused by isobaric mixing,
790 *J. Atmos. Sci.*, 57, 1675–1685, 2000.

791 Korolev, A. V. and I.P. Mazin,: Supersaturation of water vapor in clouds. *J. Atmos. Sci.*, 60, 2957-
792 2974, 2003.

793 Krueger, S., Su, C.-W., and McMurtry, P.: Modeling entrainment and finescale mixing in cumulus
794 clouds, *J. Atmos. Sci.*, 54, 2697–2712, 1997.

795 Kumar, B., Schumacher, J., and Shaw, R. A.: Cloud microphysical effects of turbulent mixing and
796 entrainment, *Theor. Comput. Fluid Dyn.*, 27, 361–376, 2013.

797 Lasher-Trapp, S. G., Cooper, W. A., and Blyth, A. M.: Broadening of droplet size distributions from
798 entrainment and mixing in a cumulus cloud, *Q. J. Roy. Meteor. Soc.*, 131, 195–220, 2005.

799 Latham, J. and Reed, R. L.: Laboratory studies of the effects of mixing on the evolution of cloud
800 droplet spectra, *Q. J. Roy. Meteor. Soc.*, 103, 297–306, 1977.

801 Lehmann, K., Siebert, H., and Shaw, R. A.: Homogeneous and inhomogeneous mixing in cumulus
802 clouds: dependence on local turbulence structure, *J. Atmos. Sci.*, 66, 3641–3659, 2009.

803 Leon, D. C., French, J. R., Lasher-Trapp, S., Blyth, A. M., Abel, S. J., Ballard, S., Bennett, L. J.,
804 Bower, K., Brooks, B., Brown, P., Choulaton, T., Clark, P., Collier, C., Crosier, J., Cui, Z.,
805 Dufton, D., Eagle, C., Flynn, M. J., Gallagher, M., Hanley, K., Huang, Y., Kitchen, M., Korolev,
806 A., Lean, H., Liu, Z., Marsham, J., Moser, D., Nicol, J., Norton, E. G., Plummer, D. Price, J.,
807 Ricketts, H., Roberts, N., Rosenberg, P. D., Taylor, J. W., Williams, P. I., and Young, G.: The
808 Convective Precipitation Experiment (COPE): investigating the origins of heavy precipitation in
809 the southwestern UK, *B. Am. Meteorol. Soc.*, in press, 2016.

810 Lu, C., and Liu Y., Niu, S.: Examination of turbulent entrainment mixing mechanisms using a
811 combined approach. *J. Geoph. Res.*, 116, D20207, 2011.

812 [Lu, C., Liu, Y., S. Niu, S., and Endo, S.: Scale dependence of entrainment-mixing mechanisms in
813 cumulus clouds, *J. Geophys. Res. Atmos.*, 119, 13,877-13,890, doi:10.1002/2014JD022265, 1014](#)

814 Paluch, I. R.: Mixing and the droplet size spectrum: generalizations from the CCOPE data, *J. Atmos.*
815 *Sci.*, 43, 1984–1993, 1986.

816 Paluch, I. R. and Baumgardner, D. G.: Entrainment and fine-scale mixing in a continental convective
817 cloud, *J. Atmos. Sci.*, 46, 261–278, 1989.

818 Paluch, I. R. and Knight, C. A.: Mixing and evolution of cloud droplet size spectra in a vigorous
819 continental cumulus, *J. Atmos. Sci.*, 41, 1801–1815, 1984.

820 [Pinsky, M., Khain, A., Korolev, A., and Magaritz-Ronen, L.: Theoretical investigation of mixing in
821 warm clouds – Part 2: Homogeneous mixing, *Atmos. Chem. Phys. Discuss.*, 15, 30269-30320,
822 doi:10.5194/acpd-15-30269-2015, 20152016.](#)

823 Pinsky, M., Khain, A., and Korolev, A.: Theoretical analysis of mixing in liquid clouds – Part 3:
824 Inhomogeneous mixing, *Atmos. Chem. Phys. Discuss.*, 15, 30321–30381, doi:10.5194/acpd-15-
825 30321-2015, ~~2015~~2016.

826 Rogers, R. R.: *A Short Course in Cloud Physics*, Pergamon press, Oxford, 227 pp., 1976.

827 Squires, P.: The growth of cloud drops by condensation. *Aust. J. Sci. Res.*, 5, 66–86, 1952.

828 Su, C.-W., Krueger, S. K., McMurtry, P. A., and Austin, P. H.: Linear eddy modeling of droplet
829 spectral evolution during entrainment and mixing in cumulus clouds, *Atmos. Res.*, 47-48, 41-58,
830 1998.

831 Tolle, M. H., and S. K. Krueger, Effects of entrainment and mixing on droplet size distributions in
832 warm cumulus clouds, *J. Adv. Model. Earth Syst.*, 6, 281–299, doi:10.1002/ 2012MS000209,
833 2014.

Formatted: Font color: Black

834 **Table 1**
835 **List of Symbols**

Symbol	Description	Units
A_2	$\frac{pR_v}{e_s R_a} + \frac{L^2}{c_{pa} R_v T^2}$	-
a	$\frac{e_s R_a L^2}{p c_{pa} R_v T^2}$	-
b	$\frac{c_{pa} R_v T^2}{L^2}$	-
c_{pa}	specific heat capacity of dry air at constant pressure	$\text{J kg}^{-1}\text{K}^{-1}$
c_{pv}	specific heat capacity of water vapor at constant pressure	$\text{J kg}^{-1}\text{K}^{-1}$
\bar{D}	mean droplet diameter	m
D_2	mean square droplet diameter	m
D_v	mean volume droplet diameter	m
e	water vapor pressure	N m^{-2}
e_1	initial water vapor pressure in the cloud parcel	N m^{-2}
e_2	initial water vapor pressure in the entrained sub-saturated parcel	N m^{-2}
e_s	saturation vapor pressure above flat surface of water	N m^{-2}
$f(D)$	size distribution of cloud droplets normalized on unity	m^{-1}
L	latent heat for liquid water	J kg^{-1}
M_n	n -th moment of the droplet size distribution $\frac{\int_0^{\infty} f(r)r^n dr}{\int_0^{\infty} f(r)dr}$	m^n
N	concentration of droplets	m^{-3}
N_1	concentration of droplets before mixing	m^{-3}
p	pressure of moist air	N m^{-2}
R_a	specific gas constant of moist air	$\text{J kg}^{-1}\text{K}^{-1}$
R_v	specific gas constant of water vapor	$\text{J kg}^{-1}\text{K}^{-1}$
RH	e/E_s , relative humidity over water (saturation ratio)	-

Formatted Table

RH_1	initial relative humidity in the cloud volume ($RH_1=1$)	-
RH_2	relative humidity in the entrained sub-saturated parcel	-
RH_{m0}	relative humidity after instant mixing of cloudy and entrained air, but before droplets evaporation	-
q	cloud liquid water mixing ratio (mass of liquid water per 1kg of dry air)	-
q_1	cloud liquid water mixing ratio before mixing	-
q_v	water vapor mixing ratio (mass of water vapor per 1kg of dry air)	-
S	$e/e_s - 1$, supersaturation	-
S_2	supersaturation of the dry out-of-cloud air	-
S_{m0}	supersaturation after instant mixing of cloudy and entrained air, but before droplets start evaporating	-
T	temperature	K
T_1	temperature of the cloud parcel before mixing	K
T_2	temperature of the entrained sub-saturated parcel before mixing	K
T_{m0}	temperature of the parcel after vapor mixing, but before droplet evaporation	K
β	extinction coefficient	m^{-1}
β_1	extinction coefficient before mixing	m^{-1}
δq_m	mixing ratio of liquid water required to saturate 1kg of the cloud volume after instant mixing, but before droplet evaporation.	-
δq^*	mixing ratio of liquid water required to saturate 1kg of the dry out-of-cloud air	-
μ	cloud fraction of mixing air, $0 \leq \mu \leq 1$	-
μ_{cr}	critical cloud fraction, such that for $\mu \leq \mu_{cr}$ all droplets evaporate	-
ρ_a	density of the dry air	$kg\ m^{-3}$
ρ_w	density of liquid water	$kg\ m^{-3}$
ξ	coefficient $0 \leq \xi \leq 1$ characterizing proximity of homogeneous mixing to inhomogeneous (when $\xi \rightarrow 0$).	-

837 **Figure Captions**

838 **Figure 1.** Classical conceptual diagram of (a) inhomogeneous and (b) homogeneous mixing. 1 initial
839 state; 2 mixing state; 3 final state.

840 **Figure 2.** Dependence of critical mixing fraction μ_{cr} versus mixing ratio q_0 calculated from Eq.(7).
841 Circles indicate modeled points. The calculations were performed for $T=0C$ and $H=3000m$.

842 **Figure 3.** Dependence of ξ versus μ . Numbers are the dimensionless ratios $\delta q^*/q_1$. Critical mixing
843 ratios μ_{cr} are indicated by stars. Grey area indicates the area where the moments of
844 homogeneous and extreme inhomogeneous mixing may not be segregated from in-situ
845 measurements. Dashed line was calculated for the cloud in Figs.13-14.

846 **Figure 4.** Simulation of (a) liquid water mixing ratio, (b) droplet number concentration, (c) integral
847 droplet diameter, (d) extinction coefficient, (e) mean volume diameter, (f) time of phase
848 relaxation, (g) relative humidity in the mixed volume before droplet evaporation RH_{m0} and
849 at the equilibrium state RH_m , (h) final temperature T_{m0} versus ratio of mixing μ formed
850 after homogeneous and extreme inhomogeneous mixing between dry and cloudy parcel with
851 monodisperse droplets. Black stars indicate critical mixing fraction μ_{cr} calculated from
852 Eq.(7). The calculations were performed for $RH_2 = 0.2, 0.5, 0.8, 0.95$; $D_1=20\mu m$,
853 $N_1=500cm^{-3}$; $T_1 = T_2 = 0C$; $H=1000m$.

854 **Figure 5.** Dependence of normalized liquid water mixing ratio q/q_1 (a,d,g), extinction coefficient
855 β/β_1 (b,e,h) and mean volume diameter D_v/D_{v1} (c,f,j) versus normalized number
856 concentration N/N_1 for various humidity of the entrained air (a,b,c), for various liquid water
857 mixing ratios (d,e,f) and for various temperatures (g,h,j). The calculations were performed
858 the initial conditions: $H=1000m$, $D_1=20\mu m$; for (a-c; g-j) $T_1 = T_2 = 0C$, $N_1=500cm^{-3}$; for
859 (d-f) $T_1 = T_2 = 0C$, $RH_2 = 0.5$; (g-j) $T_1 = T_2 = T_2$, $N_1=500cm^{-3}$, $RH_2 = 0.5$.

860 **Figure 6.** Simulation of (a) droplet number concentration and (b) liquid water mixing ratio, (c)
861 integral droplet diameter, (d) extinction coefficient, (e) mean volume diameter, (f) time of
862 phase relaxation, (g) relative humidity in the mixed volume before droplet evaporation
863 RH_{m0} and at the equilibrium state RH_m , (h) final temperature T_m versus ratio of mixing μ
864 formed after homogeneous and extreme inhomogeneous mixing between dry and cloudy
865 parcel with monodisperse droplets. The calculations were performed for $RH_2=0.9$;
866 $D_1=10\mu m$, $N_1=500cm^{-3}$; $T_1 = 0C$; $T_2 = -10C, -5C, 0C$; $H=1000m$.

867 **Figure 7.** Effect of temperature difference between cloud and entrained air on mixing. The
868 calculations were performed for initial temperatures T_2 : (1) -10C; (2) -5C; (3) 0C. Grey
869 circles indicate ~~extremely~~extreme inhomogeneous mixing on line 1 at the AB interval. The
870 rest cases on ~~extremely~~extreme inhomogeneous mixing are indicated by open circles. The
871 initial conditions used for the calculations were: $H=1000\text{m}$, $RH_2=90\%$; $D_1=10\mu\text{m}$,
872 $N_1=500\text{cm}^{-3}$, $T_1=0\text{C}$.

873 **Figure 8.** Conceptual diagram of cascade mixing of the out-of-cloud entrained parcel with the cloudy
874 environment

875 **Figure 9.** Simulation of stochastic mixing corresponding to stages 1-4 as indicated in Fig.8. Solid
876 red lines indicate the normalized dependences q , β , D_v vs. N for the primary stage of
877 homogeneous mixing. Dashed red lines indicate the same dependences for inhomogeneous
878 mixing. The initial conditions used for the simulations were: $H=1000\text{m}$, $T_1 = T_2 = 0\text{C}$;
879 $RH_2=0.5$; $D_1 = 10\mu\text{m}$, $N_1 = 500\text{cm}^{-3}$.

880 **Figure 10.** Conceptual diagram explaining breaking the functional relationships between the
881 microphysical moment during progressive missing (see text).

882 **Figure 11.** Droplet size distributions formed during the progressive homogeneous mixing
883 corresponding to the (a,e) primary stage; (b,f) 2nd stage; (c,g) 3rd stage; (d,h) 4th stage. Left
884 column (a,b,c,d) corresponds to the case, when the cloud temperature is equal to the dry air
885 temperature $T_1 = T_2 = 0^\circ\text{C}$.; right column (e,f,g,h) corresponds to the case when $T_1 = 0^\circ\text{C}$,
886 $T_2 = -10^\circ\text{C}$. For both cases the simulation was performed for $D_1 = 10\mu\text{m}$; $N=500\text{cm}^{-3}$;
887 $RH_2=0.9$.

888 **Figure 12.** Conceptual diagrams of scattering of measurements of q versus N for (a) extreme
889 inhomogeneous and (b) homogeneous mixing.

890 **Figure 13.** Spatial changes of particle concentration (a), extinction coefficient (b), liquid water
891 content (c) and average and mean mass diameter (d) during transit through one of the
892 convective clouds measured by CDP. The measurements were conducted during the COPE-
893 MED project on 18 July, 2015. The sampling rate 10Hz (~10m spatial resolution).
894 $H=5500\text{m}$, $T=-12\text{C}$, $RH=0.2$.

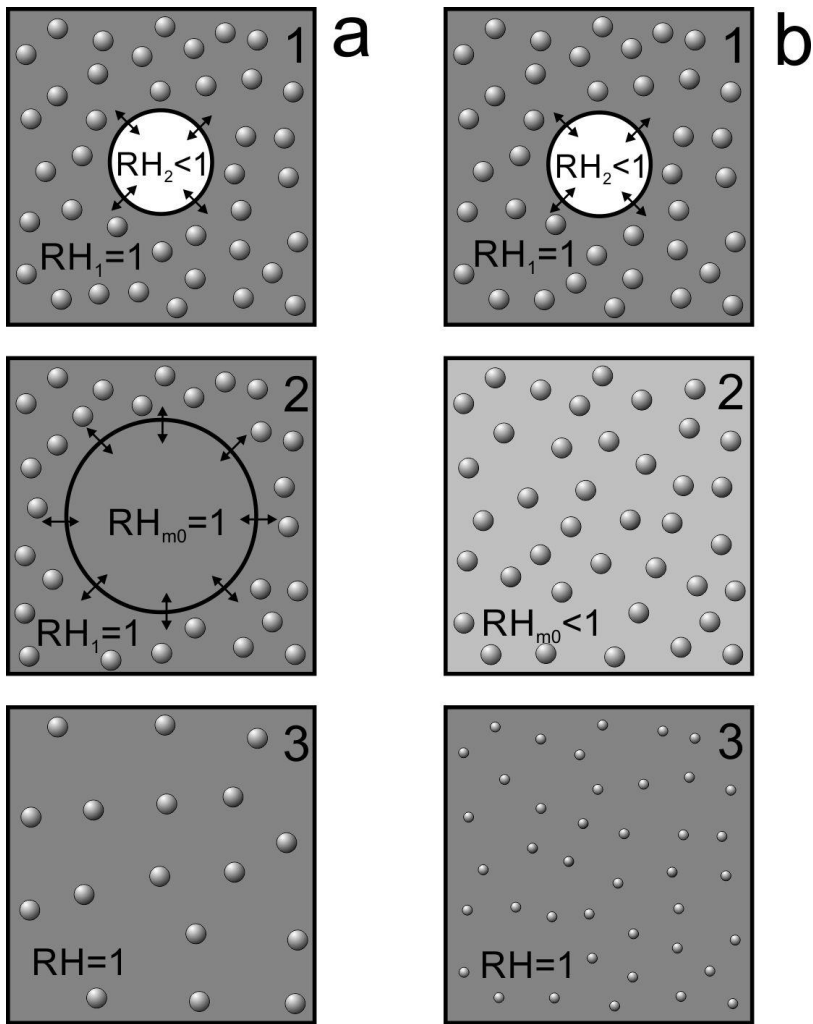
895 **Figure 14.** Relationships between (a) $LWC(N)$; (b) $\beta(N)$; (c) $D_v(N)$; (d) $LWC(\beta)$ calculated from
896 the CDP measurements obtained during sampling several convective clouds. The
897 measurements were conducted during the COPE-MED project on 18 July, 2015, $H=5500\text{m}$,

898 $T=-12\text{C}$, $RH=0.2$. The measurements were sampled at 10Hz (~10m spatial resolution).
899 Dashed lines are linear regressions. Red lines indicate primary inhomogeneous mixing
900 dependencies calculated for the same environmental conditions.

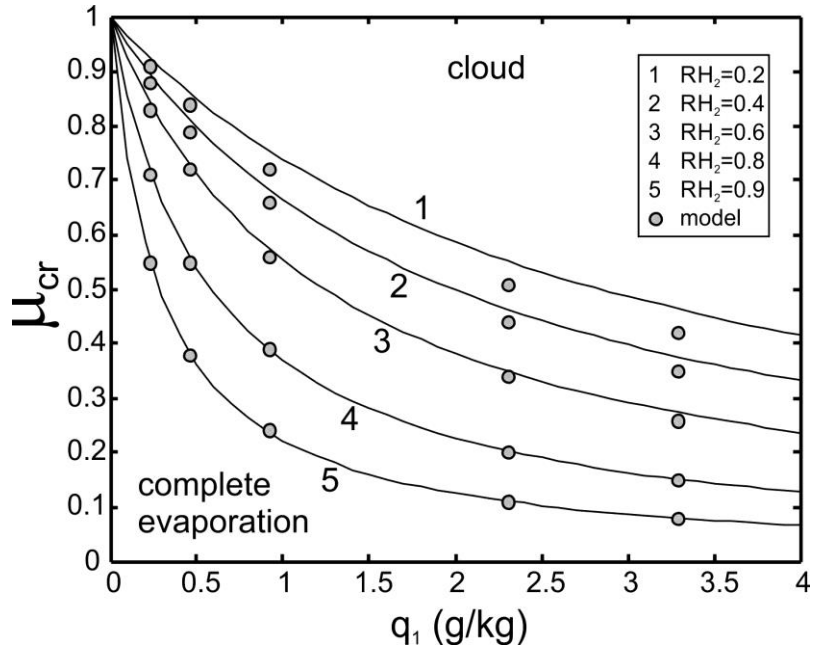
901 **Figure 15.** Relationships between (a) $LWC(N)$; (b) $\beta(N)$; (c) $D_v(N)$; (d) $LWC(\beta)$ calculated from
902 the CDP measurements sampled during traverse through 45 convective clouds. The
903 measurements were conducted during the COPE-MED project on 02 August, 2015. Dashed
904 lines indicate (a), (b) and (d) indicate the sectors, where the majority of the points are
905 scattered. The altitude of sampling varied in the range $3000\text{m} < H < 4500\text{m}$, temperature -
906 $11\text{C} < T < 0\text{C}$, relative humidity in the vicinity of clouds $15\% < RH < 65\%$. The measurements
907 were sampled at 10Hz (~10m spatial resolution).

908 **Figure A1.** Amount of evaporated liquid water δq_m required for saturation of a cloud volume with
909 initial humidity RH_m . Comparisons of the modeled δq_m and that calculated from Eqs. (A8)
910 and (A9) for three temperatures $T_{m0} = -20\text{C}$, 0C and 20C . Calculations were performed for
911 $P=880\text{mb}$.

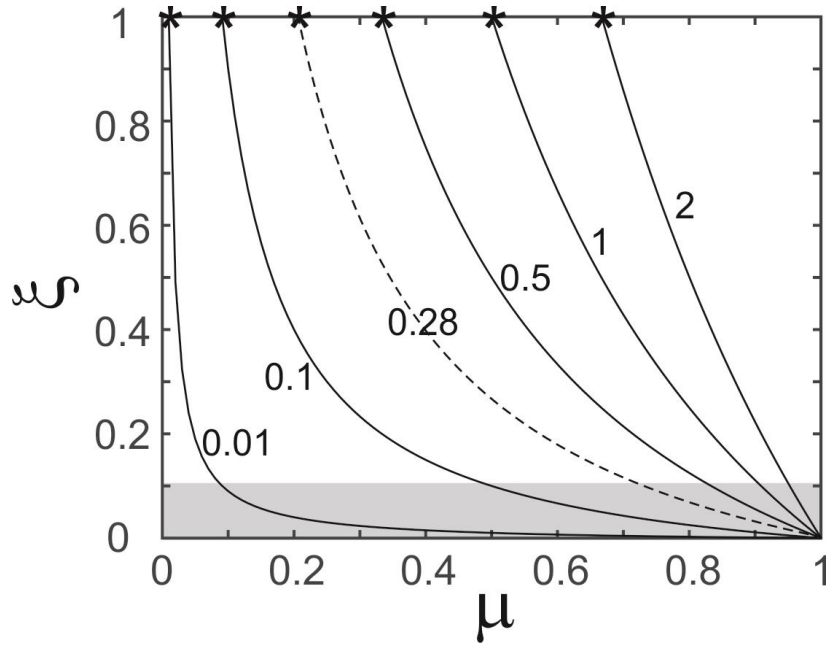
912



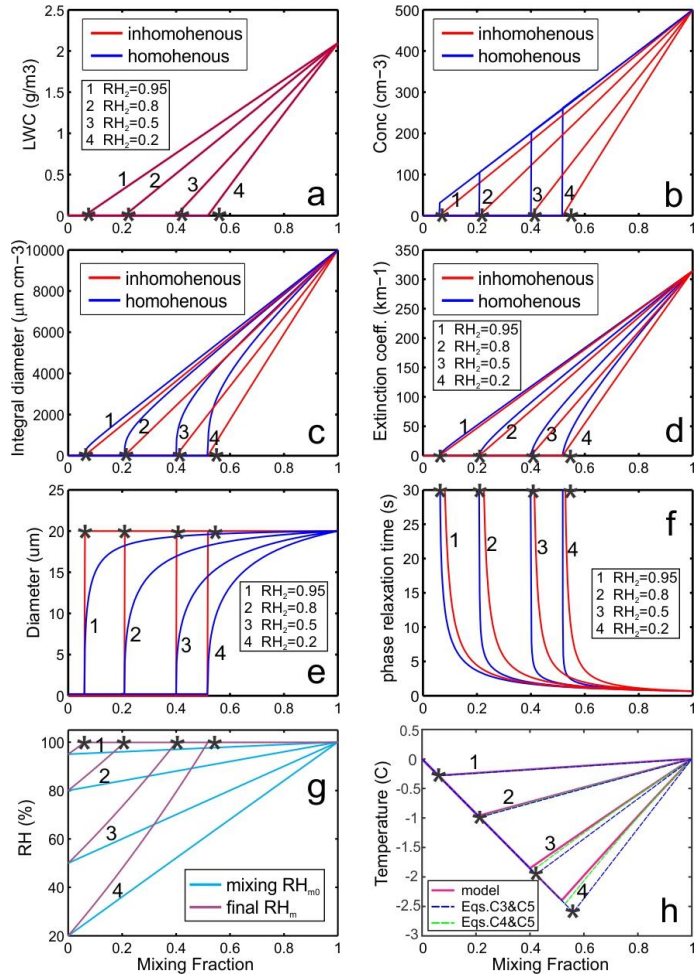
913
 914
 915 **Figure 1.** Classical conceptual diagram of (a) inhomogeneous and (b) homogeneous mixing. 1 initial state; 2
 916 mixing state; 3 final state.
 917
 918



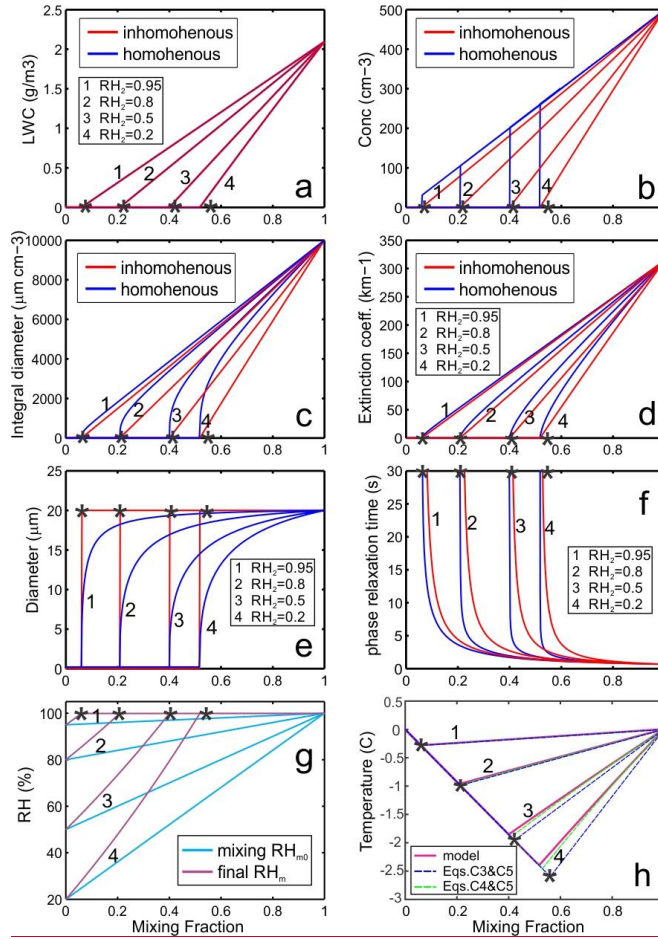
1
 2 **Figure 2.** Dependence of critical mixing fraction μ_{cr} versus mixing ratio q_0 calculated from Eq.(7). Circles
 3 indicate modeled points. The calculations were performed for $T=0C$ and $H=3000m$.
 4



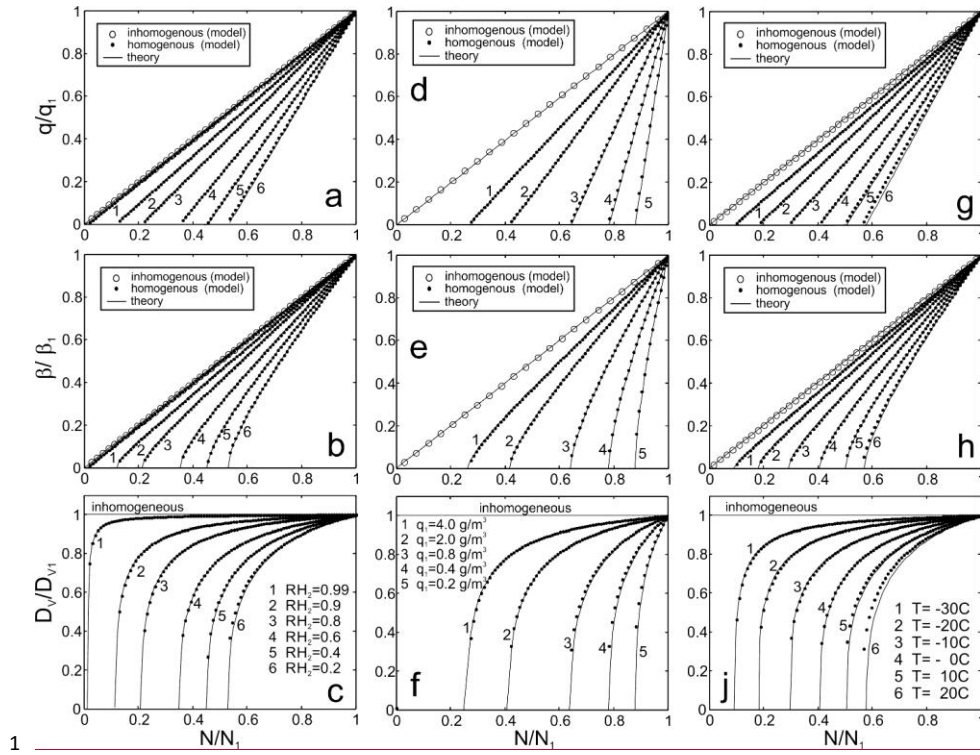
1
 2
 3 **Figure 3.** Dependence of ξ versus μ . Numbers are the dimensionless ratios $\delta q^*/q_1$. Critical mixing ratios
 4 μ_{cr} are indicated by stars. Grey ~~area~~color indicates the area where the moments of homogeneous and
 5 extreme inhomogeneous mixing may not be segregated from in-situ measurements. Dashed line was
 6 calculated for the cloud in Figs.13-14.
 7



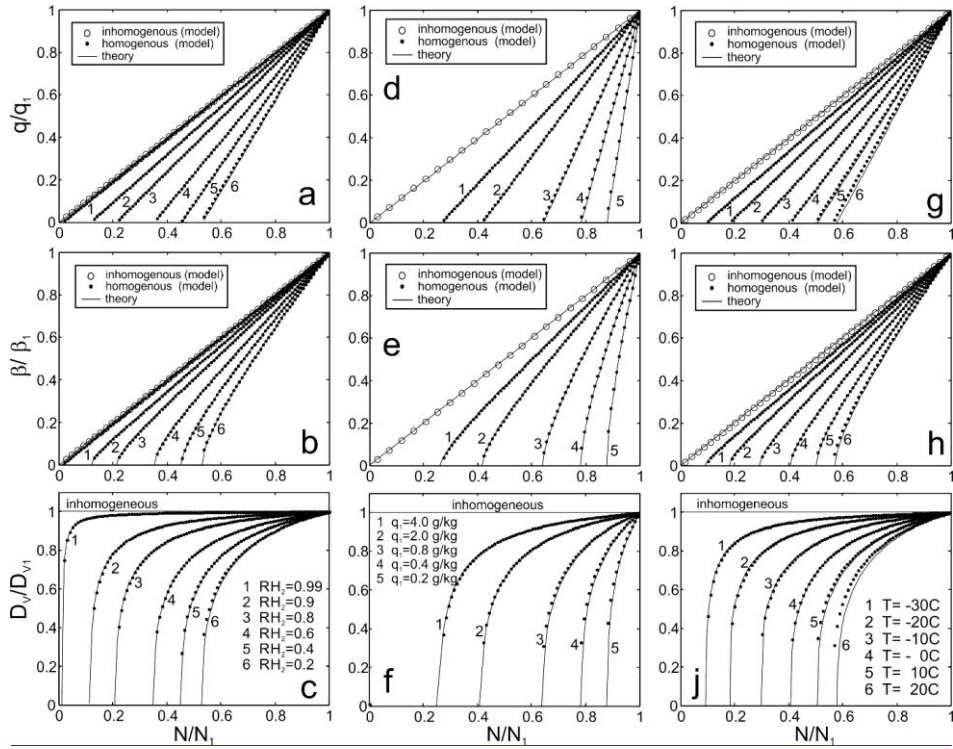
1



2
3
4 **Figure 4.** Simulation of (a) liquid water mixing ratio, (b) droplet number concentration, (c) integral droplet
5 diameter, (d) extinction coefficient, (e) mean volume diameter, (f) time of phase relaxation, (g) relative
6 humidity in the mixed volume before droplet evaporation RH_{m0} and at the equilibrium state RH_m , (h) final
7 temperature T_{m0} versus ratio of mixing μ formed after homogeneous and extreme inhomogeneous mixing
8 between dry and cloudy parcel with monodisperse droplets. Black stars indicate critical mixing fraction
9 μ_{cr} calculated from Eq.(7). The calculations were performed for $RH_2 = 0.2, 0.5, 0.8, 0.95$; $D_1=20\mu\text{m}$,
10 $N_1=500\text{cm}^{-3}$; $T_1 = T_2 = 0\text{C}$; $H=1000\text{m}$.

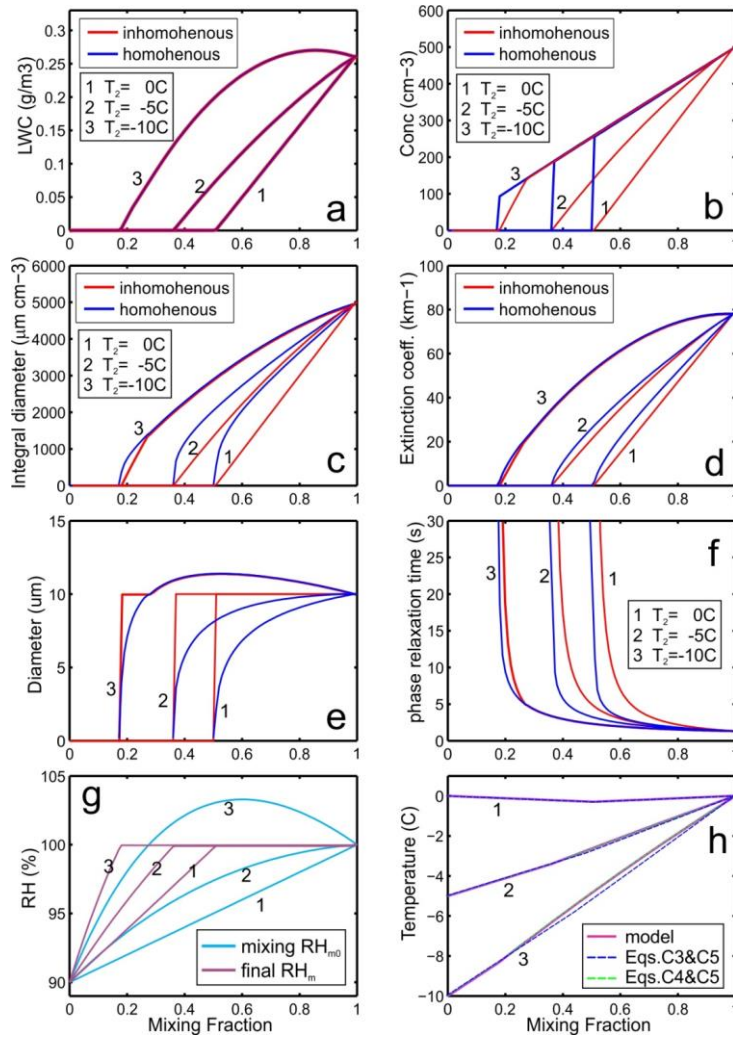


1

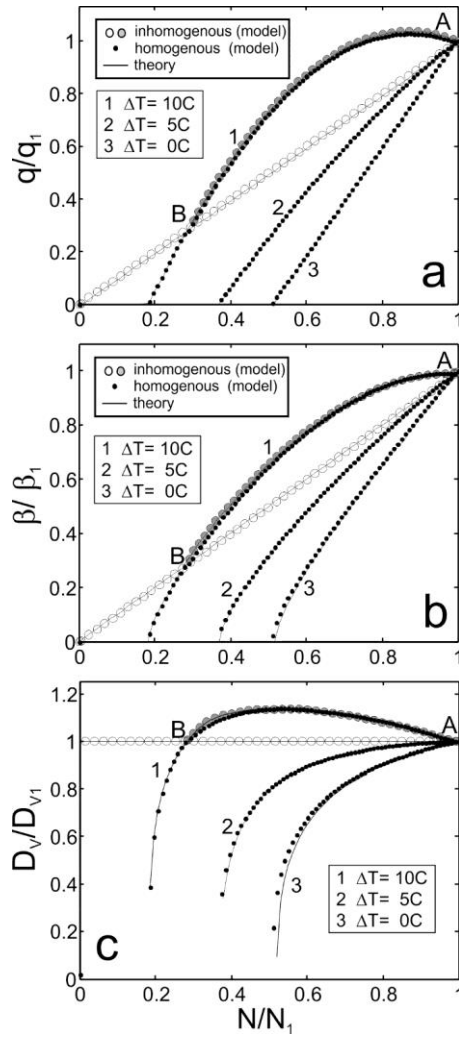


2
3
4 **Figure 5.** Dependence of normalized liquid water mixing ratio q/q_1 (a,d,g), extinction coefficient β/β_1
5 (b,e,h) and mean volume diameter D_v/D_{v1} (c,f,j) versus normalized number concentration N/N_1 for
6 various humidity of the entrained air (a,b,c), for various liquid water mixing ratios (d,e,f) and for various
7 temperatures (g,h,j). The calculations were performed the initial conditions: $H=1000\text{m}$, $D_1=20\mu\text{m}$; for (a-
8 c-g-j) $T_1 = T_2 = 0\text{C}$, $N_1=500\text{cm}^{-3}$; for (d-f) $T_1 = T_2 = 0\text{C}$, $RH_2 = 0.5$; (g-j) $T_1 = T_2 = T$,
9 $N_1=500\text{cm}^{-3}$, $RH_2 = 0.5$.

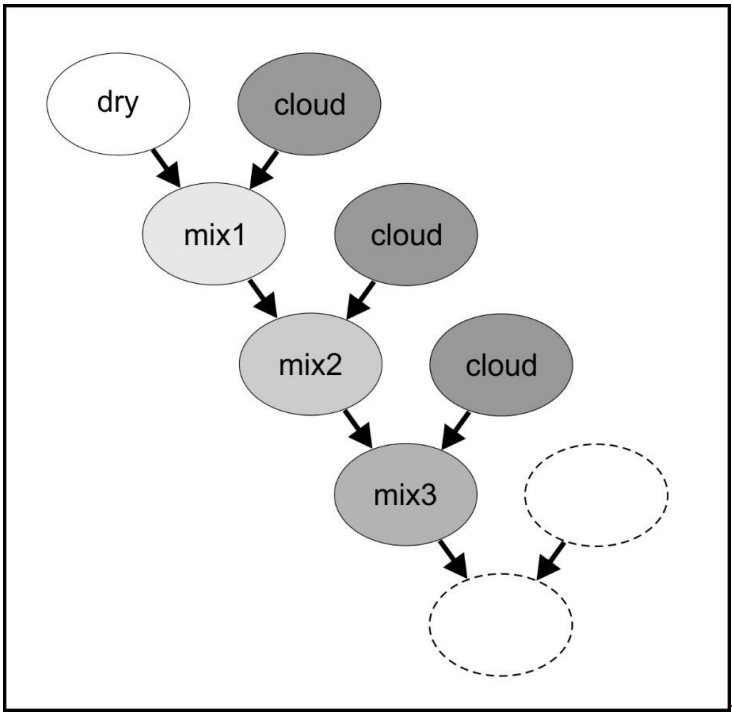
10



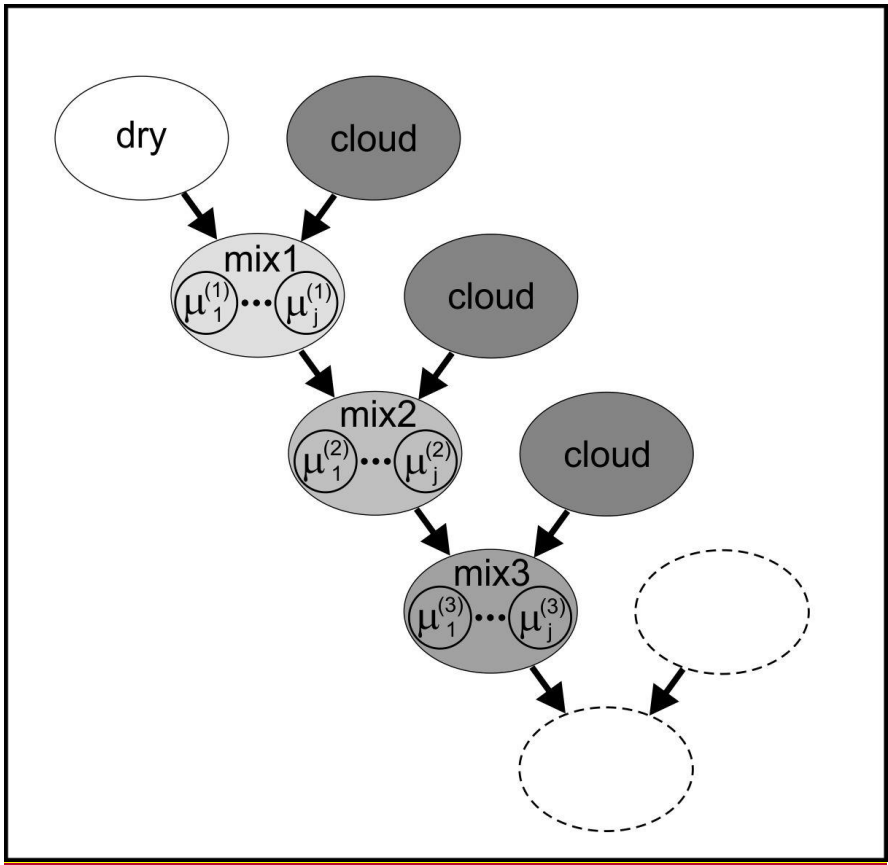
1
2
3 **Figure 6.** Simulation of (a) droplet number concentration and (b) liquid water mixing ratio, (c) integral
4 droplet diameter, (d) extinction coefficient, (e) mean volume diameter, (f) time of phase relaxation, (g)
5 relative humidity in the mixed volume before droplet evaporation RH_{m0} and at the equilibrium state RH_m ,
6 (h) final temperature T_m versus ratio of mixing μ formed after homogeneous and extreme inhomogeneous
7 mixing between dry and cloudy parcel with monodisperse droplets. The calculations were performed for
8 $RH_2=0.9$; $D_1=10\mu\text{m}$, $N_1=500\text{cm}^{-3}$; $T_1 = 0\text{C}$; $T_2 = -10\text{C}$, -5C , 0C ; $H=1000\text{m}$.



1
 2
 3 **Figure 7.** Effect of temperature difference between cloud and entrained air on mixing. The calculations were
 4 performed for initial temperatures T_2 : (1) -10C; (2) -5C; (3) 0C. Grey circles indicate extremely extreme
 5 inhomogeneous mixing on line 1 at the AB interval. The rest cases on extremely extreme inhomogeneous
 6 mixing are indicated by open circles. The initial conditions used for the calculations were: $H=1000m$,
 7 $RH_2=90\%$; $D_1 = 10\mu m$, $N_1 = 500cm^{-3}$, $T_1=0C$.

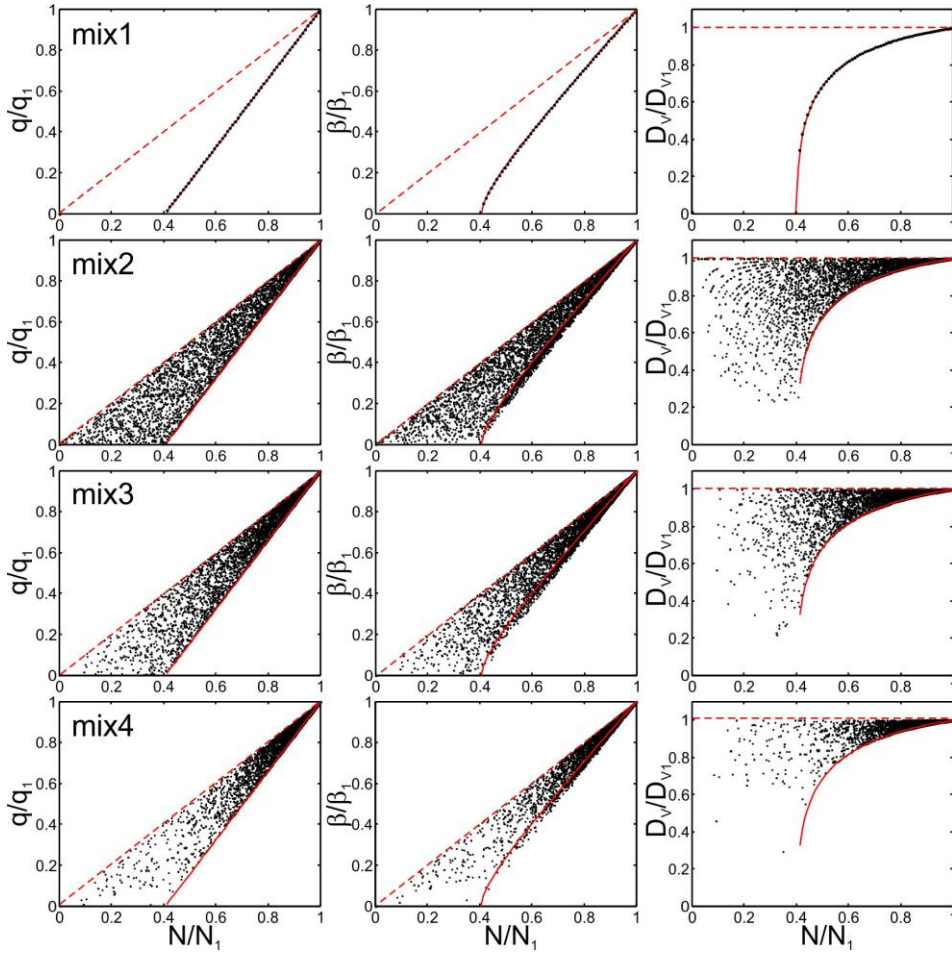


1



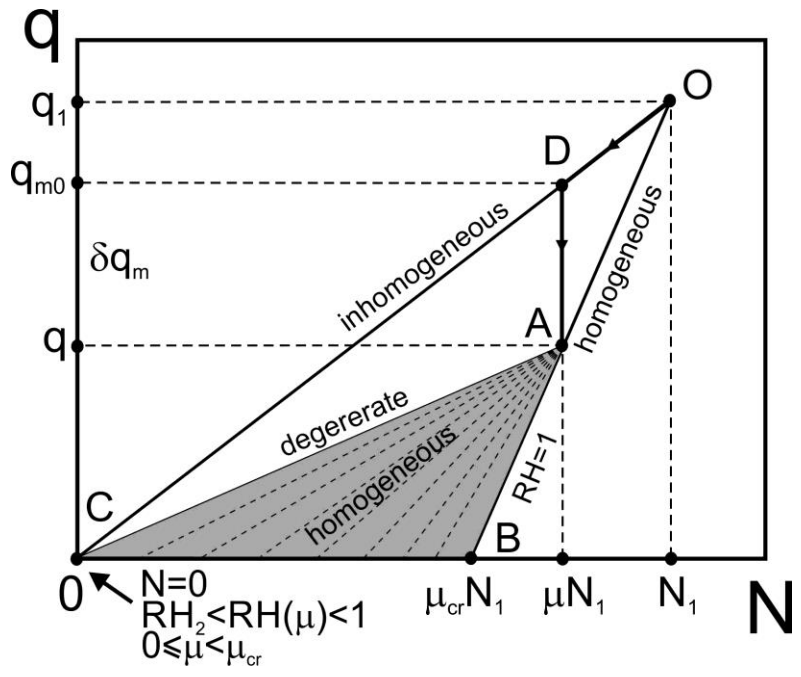
2
3
4
5
6
7

Figure 8. Conceptual diagram of cascade mixing of the out-of-cloud entrained parcel with the cloudy environment.



8
 9 **Figure 9.** Simulation of stochastic mixing corresponding to stages 1-4 as indicated in Fig.8. Solid red lines
 10 indicate the normalized dependences q , β , D_v vs. N for the primary stage of homogeneous mixing. Dashed
 11 red lines indicate the same dependences for inhomogeneous mixing. The initial conditions used for the
 12 simulations were: $H=1000\text{m}$, $T_1 = T_2 = 0\text{C}$; $RH_2=0.5$; $D_1 = 10\mu\text{m}$, $N_1 = 500\text{cm}^{-3}$.

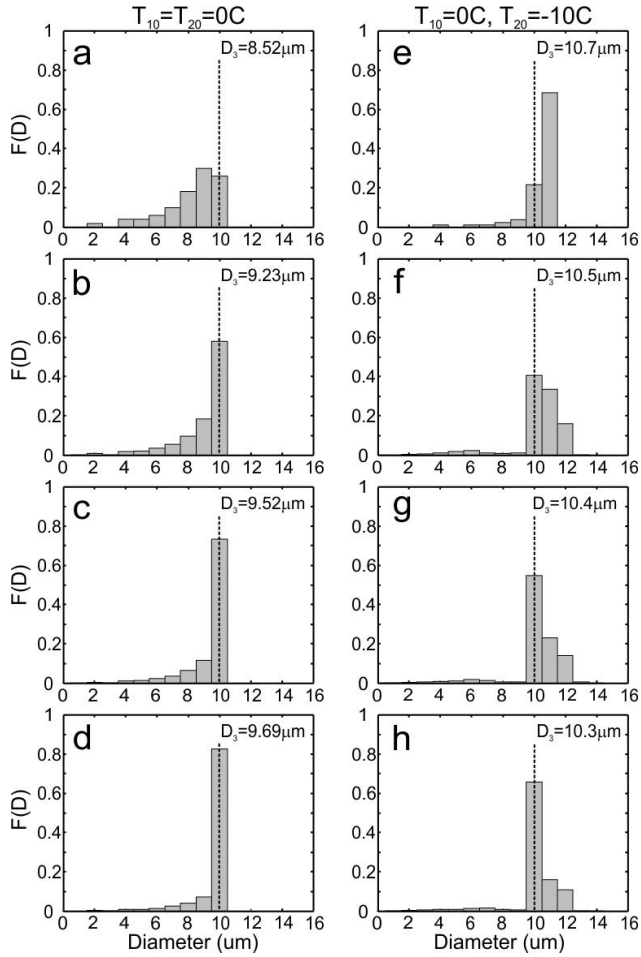
13



1
2
3
4
5

Figure 10. Conceptual diagram explaining breaking the functional relationships between the microphysical moment during progressive missing (see text).

1



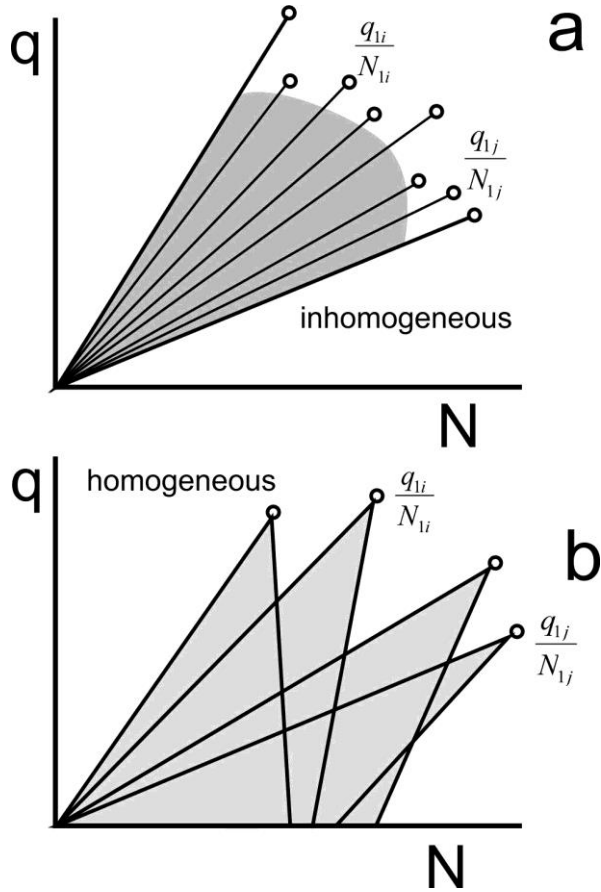
2

3

4 **Figure 11.** Droplet size distributions formed during the progressive homogeneous mixing corresponding
5 to the (a,e) primary stage; (b,f) 2nd stage; (c,g) 3rd stage; (d,h) 4th stage. Left column (a,b,c,d) corresponds
6 to the case, when the cloud temperature is equal to the dry air temperature $T_1 = T_2 = 0\text{C}$.; right column
7 (e,f,g,h) corresponds to the case when $T_1 = 0\text{C}, T_2 = -10\text{C}$. For both cases the simulation was performed
8 for $D_1 = 10\mu\text{m}; N=500\text{cm}^{-3}; RH_2=0.9$.

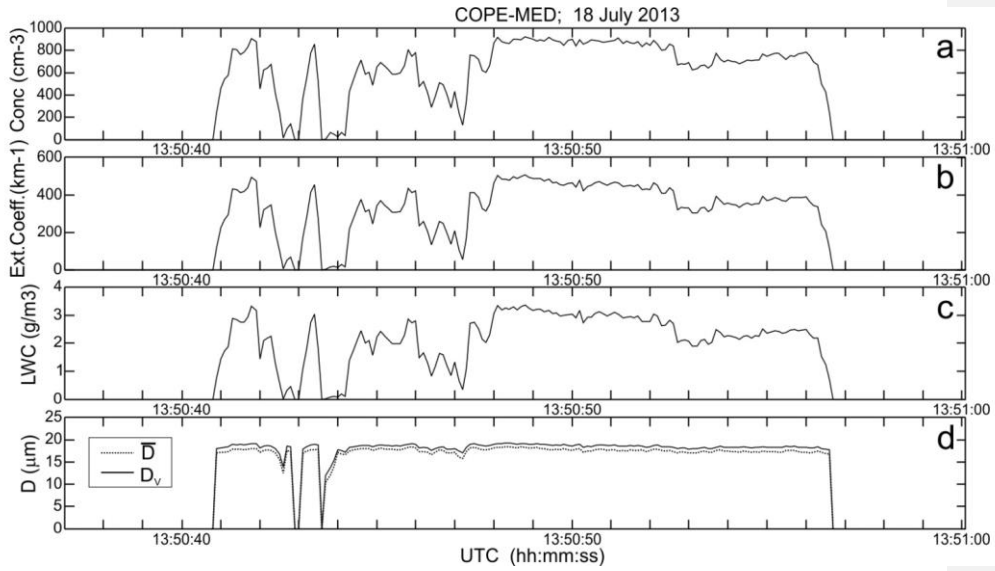
9

1
2

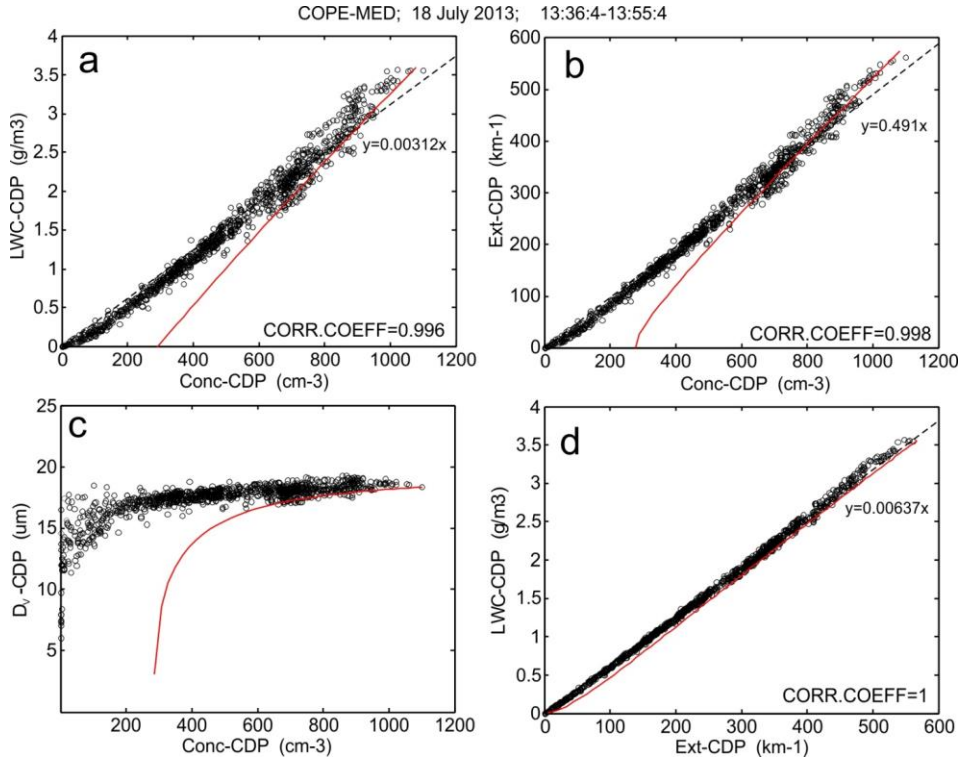


3
4
5
6
7
8

Figure 12. Conceptual diagrams of scattering of measurements of q versus N for (a) extreme inhomogeneous and (b) homogeneous mixing.

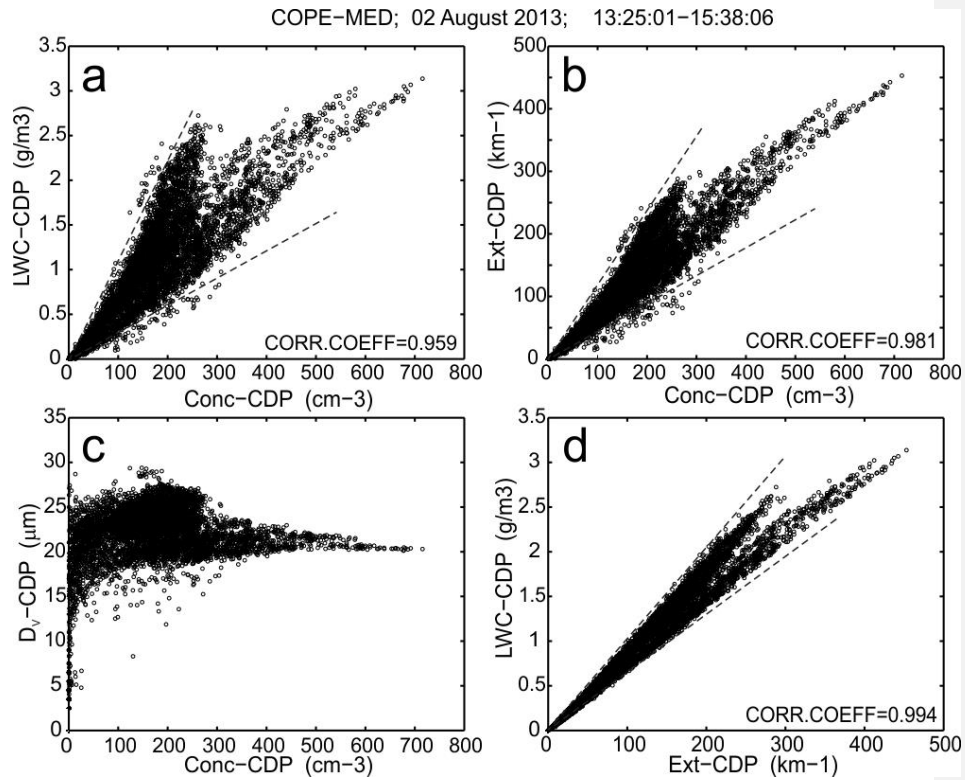


1
 2 **Figure 13.** Spatial changes of particle concentration (a), extinction coefficient (b), liquid water content (c)
 3 and average and mean mass diameter (d) during transit through one of the convective clouds measured by
 4 CDP. The measurements were conducted during the COPE-MED project on 18 July, 2015. The sampling
 5 rate 10Hz (~10m spatial resolution). $H=5500\text{m}$, $T=-12\text{C}$, $RH=0.2$.
 6



1
2
3
4
5
6
7
8
9
10

Figure 14. Relationships between (a) $LWC(N)$; (b) $\beta(N)$; (c) $D_v(N)$; (d) $LWC(\beta)$ calculated from the CDP measurements obtained during sampling several convective clouds. The measurements were conducted during the COPE-MED project on 18 July, 2015, $H=5500\text{m}$, $T=-12\text{C}$, $RH=0.2$. The measurements were sampled at 10Hz ($\sim 10\text{m}$ spatial resolution). Dashed lines are linear regressions. Red lines indicate primary inhomogeneous mixing dependencies calculated for the same environmental conditions.



1
2
3
4
5
6
7
8
9
10

Figure 15. Relationships between (a) $LWC(N)$; (b) $\beta(N)$; (c) $D_v(N)$; (d) $LWC(\beta)$ calculated from the CDP measurements sampled during traverse through 45 convective clouds. The measurements were conducted during the COPE-MED project on 02 August, 2015. Dashed lines indicate (a), (b) and (d) indicate the sectors, where the majority of the points are scattered. The altitude of sampling varied in the range $3000\text{m} < H < 4500\text{m}$, temperature $-11\text{C} < T < 0\text{C}$, relative humidity in the vicinity of clouds $15\% < RH < 65\%$. The measurements were sampled at 10Hz (~10m spatial resolution).

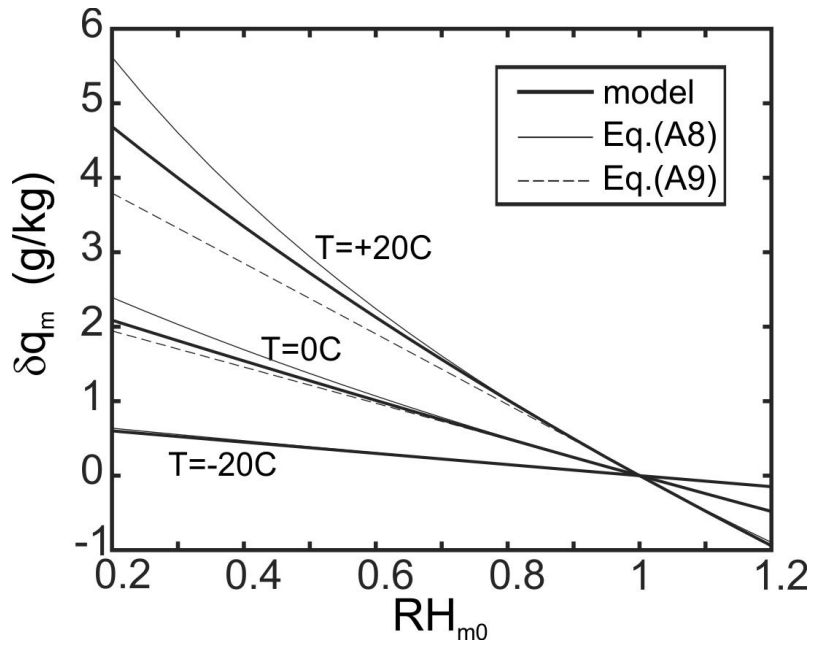


Figure A1. Amount of evaporated liquid water δq_m required for saturation of a cloud volume with initial humidity RH_m . Comparisons of the modeled δq_m and that calculated from Eqs. (A8) and (A9) for three temperatures $T_{m0} = -20\text{C}$, 0C and 20C . Calculations were performed for $P=880\text{mb}$.